Tidal dissipation from free drift sea ice in the Barents Sea assessed using GNSS beacon observations

Vasulkar, Amey; Verlaan, Martin; Slobbe, Cornelis; Kaleschke, Lars

Important note
To cite this publication, please use the final published version (if applicable).
Please check the document version above.

Tidal dissipation from free drift sea ice in the Barents Sea assessed using GNSS beacon observations

Amey Vasulkar[1,2] [ID] · Martin Verlaan[1,2] · Cornelis Slobbe[3] · Lars Kaleschke[4]

© The Author(s) 2022

Abstract

One of the major challenges facing global hydrodynamic tidal models is the modelling of the interaction between sea ice and tides in high-latitude waters. Recent studies have shown strong seasonal correlation between sea ice and tides. Hence, it is important to accurately model the effect of sea ice in a tidal model. Presence of sea ice leads to a frictional dissipation of tides. Most models either completely ignore sea ice or partly include it by assuming a fixed sea ice cover (landfast ice). However, sea ice can also be drifting and the nature of dissipation between drifting sea ice and tides is partly unknown. We assess the dissipation of tides due to free drift sea ice. In the absence of wind, this is negligible in the deeper and open ocean. For the shallow water regions, however, this dissipation is unknown. Here, we evaluate this dissipation for the Spitzbergen Shelf region using a beacon dataset showing strong free drift subdaily sea ice oscillations and a physics based point ice model. Two analyses were done which compared the model and observed motion. The analyses showed that for winds speeds below 8m/s and with low subdaily signals, the subdaily free drift sea ice motion is strongly connected to the tides and that the frictional dissipation is low. In the context of global tide and storm surge models, the dissipation from free drift sea ice on tides should be evaluated based on the region (deep ocean or shallow water) and existing wind conditions. In the presence of strong winds the dissipation between free drift sea ice and air can be significant on a subdaily scale even if there are no subdaily signals in the wind itself.

Keywords Free drift sea ice · Global tide models · Tidal sea ice interface dissipation · Ice buoys · Sea ice oscillations · Subdaily motion

1 Introduction

Hydrodynamic global tide models have improved significantly in the past couple of decades due to a combination of improved modelling and data assimilation. Yet, these models still face challenges in high-latitude waters (poleward of $\pm 66°$ latitude) (Stammer et al. 2014; Kleptsova and Pietrzak

✉ Amey Vasulkar
   a.n.vasulkar@tudelft.nl

1 Delft Institute of Applied Mathematics, TU Delft, Delft, The Netherlands

2 Deltares, Delft, the Netherlands

3 Civil Engineering and Geosciences, TU Delft, Delft, The Netherlands

4 Alfred-Wegener-Institut Helmholtz-Zentrum für Polar- und Meeresforschung, Bremerhaven, Germany

2018). Among these challenges is the fact that most of these global tidal models either completely or partly ignore the interaction between sea ice and tides. This also applies to a model we are co-developing with Deltares, named, Global Tide and Surge Model (GTSM Verlaan et al. 2015; Muis et al. 2016). Apart from global tidal models, there are some regional tidal models for the Arctic like Padman and Erofeeva (2004) and Chen et al. (2009) which perform well. Of these too, Padman and Erofeeva (2004) do not consider sea ice while the AO-FVCOM model of Chen et al. (2009) is a 3D model coupled to a sea ice model. Yet, these models are regional and are not suitable to study the effects of sea ice on tides globally.

Sea ice leads to a dissipation of tidal energy. The magnitude and nature of this energy loss is still a topic of ongoing research (Stammer et al. 2014). The friction generated by tides at the sea ice-ocean interface is a potential mechanism for this tidal energy dissipation (Kleptsova and Pietrzak 2018). The stress from this friction can be represented in a model through

a simple parameterization where the stress is proportional to the square of the relative velocity between sea ice and tidal velocity (McPhee 1982; Pease et al. 1983). Some global tidal models that partly include the sea ice assume all of the sea ice to be stationary/time-invariant (landfast ice) with annual mean state (Stammer et al. 2014). This simplifies the relative velocity to just the velocity of water/tides. But, sea ice is also drifting and the sea ice area is seasonally varying.

Recent studies (Kagan and Sofina 2010; Müller et al. 2014; Kleptsova and Pietrzak 2018; Bij de vaate et al. 2020) have shown strong seasonal correlation between sea ice and the tidal constituents. Kleptsova and Pietrzak (2018) dealt with this problem by using a monthly sea ice concentration field while assuming all the sea ice to be stationary. However, this still ignores the fact that only 12% of the northern hemisphere wintertime sea ice cover is landfast ice Mahoney (2018) while, the remaining fraction is drifting sea ice.

In the case of drifting sea ice, modelling the water-ice frictional stress requires the relative velocity between sea ice and water. To evaluate this, one would need sea ice velocities on subdaily timescales from models which include tidal forcing. Such models, if any, should be 3D ice-ocean coupled models which would correctly resolve the effect of ice on water and vice versa and should include tides. Such a dataset of sea ice velocities is not known to be publicly available and in fact, many sea ice models typically omit tidal forcings (Heil and Hibler 2002). On the other hand, remote sensing derived products provide the mean total velocities at weekly/monthly resolution so these cannot be used either. That said, most of the hydrodynamic tide models are 2D and in these models it would suffice to include an efficient parameterization of the frictional dissipation from drifting sea ice on tides.

It is unknown how much drifting sea ice contributes to the dissipation of tides. The work of Kleptsova and Pietrzak (2018) suggests that the impact could be significant. In fact, integrated over a large domain even quite small dissipation at the ice-tide interface could be relevant for large scale tide modelling. Our long term aim is to estimate the amount of energy loss between drifting sea ice and tides and if significant find a parameterization that can be used in global tide models. To estimate the energy loss, it is important to understand the interaction between the drifting sea ice motion and tides and the underlying physics.

The motion of drifting sea ice can be divided into motions at subdaily and longer time scales. The subdaily sea ice motion interacts with tides and is therefore important for our study. This subdaily motion is essentially formed by sea ice oscillations containing both inertial oscillations, attributed to inertial forcing (coriolis force) (Hunkins 1967; McPhee 1978), and tidal oscillations (Pease et al. 1995; Heil and Hibler 2002). The proportion of inertial or tidal component in the oscillations helps evaluate the relative motion between sea ice and tides. There are a few regional studies (Pease et al. 1995; Hibler et al. 2006; Kowalik and Proshutinsky

1994) which investigated the interaction between the subdaily sea ice drift and tides. All these studies were performed to study the effect of tides on sea ice drift and deformation and not vice versa, i.e., the effect of sea ice on the dissipation of tides. Nevertheless, they shed light on the nature of the subdaily sea ice motion and its relationship with tides.

Pease et al. (1995) in their harmonic analysis of the Argos buoys in the Barents Sea continental shelf region observed that the M_2 tidal constituent in the subdaily sea ice motion was a magnitude larger than the inertial oscillation. Also, Kowalik and Proshutinsky (1994) using their model for the Arctic Central Basin noted that the subdaily sea ice motion is dominated by tides but not inertial forces. This was in contrast to Hibler et al. (2006) who, using a sea ice model proposed by Heil and Hibler (2002), showed that in the subdaily sea ice oscillations of the Arctic Central basin, the inertial effects dominate and are enhanced by tidal forcing. This contradiction could be attributed to the different sea ice models used by Kowalik and Proshutinsky (1994) and Hibler et al. (2006). While Pease et al. (1995) and Kowalik and Proshutinsky (1994) had similar conclusions of tides being a dominant aspect of subdaily sea ice motion, the relative magnitude of inertial oscillations in both the studies was different. The difference here, might be a result of different magnitudes of internal stresses in the drifting ice field in the central Arctic and the Barents Sea region. This adds to the complexity as drifting sea ice field with and without significant internal stresses and based on the region of the Arctic could have different dissipation on the tides.

On this context, we propose to divide the sea ice field into two regimes: sea ice drifting under strong internal stresses and under weak/no internal stresses Zubov (1945). The latter is also referred to as *free-drift* (McPhee 1980). Consequently, the interaction of each regime with tides needs to be studied separately. In this paper, we only consider free drift sea ice field and its dissipation on tides thereof.

It is noted in McPhee (1978); Leppäranta and Leppäranta (2011b) that in free drift and no-wind conditions, the sea ice and water velocities are equal under steady state. This implies that there will be no dissipation at the sea ice-tide interface. In fact, under low winds with no subdaily signal too, it can be seen that such a dissipation is negligible (Omstedt et al. 1996). But these analyses assumed deep and open oceans. It is not clear whether and how strong the dissipation is in case of strong winds or in shallow water regions (i.e. depths< 50 m) where the bottom friction is significant or in straits where vorticity of the current is affected.

Here, we focus on studying the dissipation in scenarios of shallow water regions and strong winds. For this study, we have GNSS observations of beacons in a free drift sea ice field showing sea ice oscillations at a temporal resolution of 15 min in the shallow water region of the Barents Sea, south-east of Svalbard. Moreover the tides are also strong in this region.

Our aim is to analyse the oscillations from this dataset and assess the dissipation of tides due to free drifting sea ice in such shallow water region. This analysis would give us a methodology which could help in assessing such dissipation for the global tidal models.

Analysing the sea ice oscillations would require separating the tidal and inertial oscillations. In the Barents sea region, the semidiurnal tidal frequencies, particularly M_2, and inertial frequencies are close to each other Furevik and Foldvik (1996); Middleton and Denniss (1993). Thus, in an harmonic analysis of the time series of buoy positions, similar to Pease et al. (1995), long time series are required to separate them and satisfy the Rayleigh criterion. The beacon dataset we have, does not satisfy this requirement. Moreover the inertial frequency varies with latitude and the beacon data cannot be considered homogeneous. So, it is impossible to separate the signal from inertial and tidal parts based on their frequency alone. Hence, in this paper, a *physics-based approach* is used by developing a point ice model to help separate the inertial and tidal signals/oscillations from the subdaily free drift sea ice oscillations. From now on, these are simply referred to as *sea ice oscillations* but the reader should bear in mind that these are free drift sea ice oscillations.

Using the point ice model and observations, two analyses are presented. The first evaluates the correlation between the sea ice oscillations and the tidal currents/tides which sheds light on the relative motion between the two. The second one assesses the causality of the sea ice oscillations by performing a forcing sensitivity analysis. Here, the point ice model is used to conduct a sensitivity analysis on the sea ice oscillations from the forcing in the model and in effect, determine the significant cause of the sea ice oscillations. Knowing this forcing responsible for the cause of sea ice oscillation coupled with the information on relative motion between sea ice oscillations and tidal currents helps us compute the dissipation between free drift sea ice-tide interface in the shallower region of the Barents Sea and understand its significance thereof.

The paper is structured as follows: Section 2 describes the buoy observations and their validation for the free drift assumption. Following this, there is point ice model description and validation in Section 3. In Sections 4, and 5, we present and discuss the results of the two analyses. Section 6 gives insight into the energy dissipation and finally, we end by summarising the main findings and concluding remarks.

2 Buoy observations

During an experiment for testing a sea ice forecast and ship route optimisation system in the Barents Sea (Kaleschke et al. 2016) in March 2014, an array of 15 drifting ice buoys
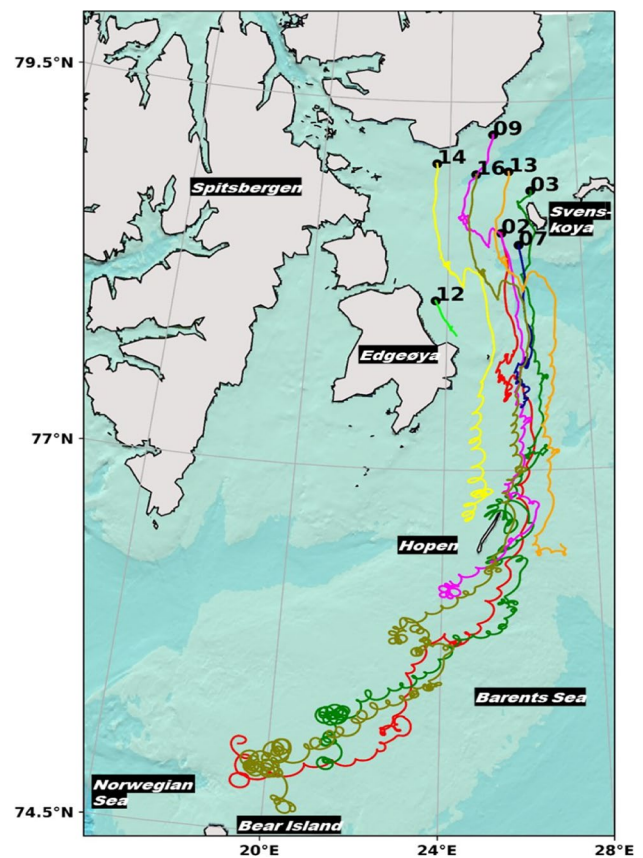

Fig. 1 The trajectories for 8 out of the 15 beacons starting from March 16. The remaining beacons were either damaged or lost after deployment. The original experiment intended for the beacons to transmit data for a period in March, but some of the beacons were even operational till the end of May

Kaleschke and Müller (2022) (beacons[1]; as they were called by their manufacturer and henceforth referred to as in this paper) were deployed from an aircraft. Their purpose was to determine the origin of the sea ice and see if the ice thickness changes are caused by ice dynamics or ice growth and melting. The beacons had an in-built GNSS receiver with the beacon positions sampled at a frequency of 15 min. Based on the beacon positions, the velocity of the beacons was computed using a forward difference scheme. The beacon trajectories (Fig. 1) started in the Barents Sea, east of Svalbard. Initially, the trajectories are seen to move south and then turn south-west over the shallow Spitsbergen bank. The clockwise loops formed by the trajectories are the sea ice oscillations, and these move in a coiled manner as the oscillations have a mean drift to the south-west.

A high correlation between these sea ice oscillation loops in beacon trajectories and the magnitude of tidal currents

---
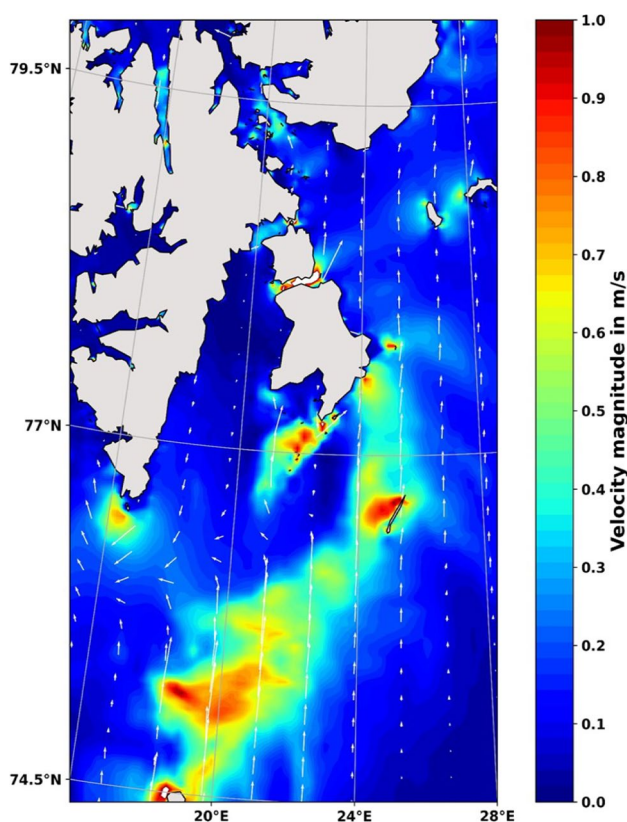
Fig. 2 Plots showing contours of tidal velocity magnitude with arrows showing the movement of tidal currents on March 31 at 00:00am. The plot is obtained by computations on GTSM. The length of the velocity vectors is scaled according the velocity magnitude

is evident from Figs. 1 and 2. Tidal currents in Fig. 2 are computed using the in-house global tidal model, GTSM, and plotted for March 31 at 00:00am. It can be said that the beacons move under strong tidal currents. These strong currents are not a result of some local time specific event but, in fact, this region of Spitsbergen bank is known to have high tidal currents (Kowalik and Untersteiner 1978; Kowalik 1979; Gjevik and Straume 1989). Thus, the oscillations observed in beacon trajectories below the 78 °N latitude in the Spitsbergen bank are a result of inertial as well tidal forces as also noted in the study of Pease et al. (1995).

The tidal currents seem to go from south to north while the beacon movements are north to south. This could be due to southwesterly winds as seen in the tidal ice dynamics study of Dmitriev et al. (1991) for the same area. In fact, Dmitriev et al. (1991) studied that under strong tidal forcing, elliptical shape traces are formed in the ice field signifying a tidal ice drift in the Marginal Ice Zone areas with ice concentration around 70%. These elliptical traces are essentially the sea ice oscillations. In our Barents Sea experiment too, these sea ice oscillations are possible in the marginal ice zone with low sea ice concentrations.

The sea ice field conditions for parts of the beacon trajectories can be found in Kaleschke et al. (2016). It is seen that,

(Fig. 3 in the reference) during the experiment, in the region between Edgeøya and Svenskoya the sea ice had high compactness with no signs of leads. This implies that in this region there were high internal stresses. In fact, the stresses were so high that the ice was (almost) stationary and some of the beacons got stuck (see beacon 12 Fig. 1). These high internal stresses could be a reason for the lack of oscillations observed in this region of the beacon trajectories. Now, as the beacons move south and start oscillating below the 78 °N latitude it is important to know the nearby sea ice concentration. Using the high resolution (3.125 km) AMSR2 daily sea ice concentration product Beitsch et al. (2014), the field of sea ice concentration is plotted for April 3 (Fig. 3) along with all, then operational, beacon (6 of the 8) trajectories.

The trajectories started from March 31 as post this date, all the beacons were well below 78 °N latitude. On April 3, the beacons are mostly in the marginal ice zones with sea ice field concentrations lower than 80%. Such zone is usually composed of relatively small ice floes and not a compact sheet and hence, the internal stresses in the ice field are low. While for the beacon 09, which appears to be in a high concentration field, the sea ice field is far away from the coast of Edgeøya or Hopen for the ice field to have any forcing from the boundaries. In such sea ice, the internal ice stresses are relatively low. That said, this argument is also valid, later in time, when the beacons move towards south west and the ice field in the region extends up to Bear Island. Although, the arguments here are based on sea ice concentration field for one day, they are valid for concentration fields on other days as well. In Online Resource 3, one can find the sea ice concentrations for other days along with the beacon trajectories and one can also compare between the AMSR2 product and another sea ice product.

Based on these arguments, we can assume that the beacons move in sea ice field having low/no internal stresses and having concentrations mostly below 80%. In such a field, a free drift can be considered as a good approximation (McPhee 1980; Leppäranta and Omstedt 1990). Consequently, in this paper, we consider the beacon trajectories starting from March 31 and assume they are free drifting.

3 Point ice model

We analyse the interaction between free drift sea ice and tides mathematically in an effort to validate the free drift equations governing the point ice model.

3.1 Mathematical analysis of governing equations

The governing equation of tides and free drift sea ice are compared. The momentum equation of tides in 2D hydrodynamic tidal models is essentially, the shallow water equations, given by:
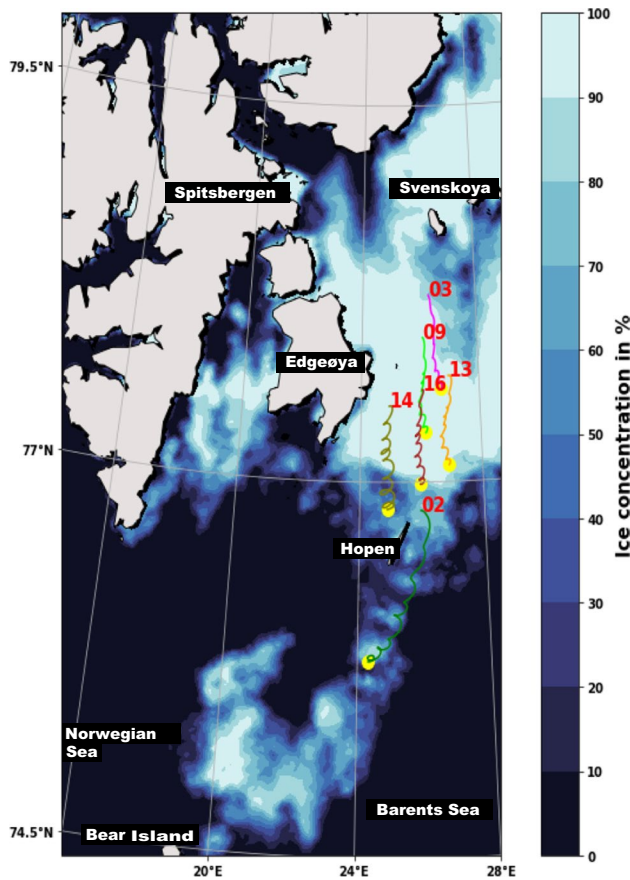
Fig. 3 Sea ice concentration obtained from the AMSR2 product for April 3. The individual beacon tracks are shown starting from March 31 with the yellow coloured markers showing the beacon positions on April 3

$$\frac{du_{wt}}{dt} + fe^{i\pi/2}u_{wt} = -g\nabla\zeta_t - \frac{\tau_b}{\rho_w H} + \nu\nabla^2 u_{wt} - \frac{\tau_{wi}}{\rho_w H}, \qquad (1)$$

where u_{wt} is the water tidal velocity vector, ρ_w is the density of water, H is the water depth, ν is the kinematic viscosity of water, $fe^{i\pi/2}$ is the complex Coriolis parameter, $g(9.81 \, \text{m/s}^2)$ is the acceleration due to gravity, τ_b is the bottom frictional stress from the sea bed, $\nabla\zeta_t$ is the pressure gradients from tidal sea surface heights and τ_{wi} is the water-ice frictional stress at ice-water interface.

On the other hand, the sea ice free drift equation (Leppäranta and Leppäranta 2011b) in density averaged form is as follows:

$$\frac{du_i}{dt} + fe^{i\pi/2}u_i = -g\nabla\zeta + \frac{\tau_{ai}}{\rho_i h_i} + \frac{\tau_{wi}}{\rho_i h_i}, \qquad (2)$$

where u_i is the ice-velocity, ρ_i is the density of sea ice, h_i is the sea ice thickness. Forcing τ_{ai} is the frictional stress between the air-ice interface and likewise, τ_{wi} is the water-ice frictional stress. $\nabla\zeta$ is the gradient of sea surface heights.

Now, in the free drift sea ice equations, the forcing from sea surface heights and relative motion between ice-water interface consists of both, the ocean general circulation and tidal component. As we are comparing to governing equation for tides, consider only the tidal oceanic forcing in the free drift Eq. 2.

Comparing Eqs. 1 and 2 shows that the Left Hand Side (LHS) are the same implying the homogeneous solutions, and consequently the inertial solutions, will be the same in both the cases.

While on the Right Hand Side (RHS), both the Eqs. 1 and 2 have similar terms apart from the bottom friction drag and diffusion term in the tidal equations and wind/air-ice drag in the ice drift equations. In deeper and open oceans, for the tidal model Eq. 1, the bottom frictional stress will be small for larger depths ($H >> 1$) and can be neglected. Furthermore, as there are no straits or regions in open oceans which can cause strong vorticity the viscous diffusion term is also negligible. On the other hand, in the case of free drift model Eq. 2, under no wind, the drag from the wind is not present.

Ultimately, in both the cases (Eqs. 1 and 2) only two terms remain on the RHS of the equations-the gradients from the sea surface heights which is same in both the cases and the water-ice frictional stress but with a different scaling based on ocean depth.

Thus, we can say that both the tidal model equations and ice drift equation are similar and can expect the sea ice drift to be similar to the tides in such a situation of deeper and open oceans. This conclusion is in accordance with McPhee (1978) who also make these simplifications.

Then, an integrated ice-ocean equation would have only the pressure gradient forcing from the sea surface heights on the RHS as the external forcing driving the ocean and sea ice together. As a result, the cause of free drift sea ice oscillations is the same as the cause of tides i.e. the gradients of sea surface heights, implying that the dissipation between sea ice and tides is non-existent.

Based on this analysis, it is clear that for shallow water regions, strong vorticity regions, like straits, and for strong winds there is a velocity difference between sea ice and tides and as such, this might lead to dissipation in the interface. Now we describe our point model in the next section.

3.2 Model formulation

To use a physics-based approach for separating the tidal and inertial signals, a point ice model was developed with free drift assumption in the Spitsbergen Shelf region. The model governing equations are given by Eq. 2. As noted in Leppäranta and Leppäranta (2011b) the air-pressure gradient term in the ice-drift is minor and can be neglected.

It should be noted that we assume a constant sea ice density of $\rho_w = 920\,\text{kg/m}^3$ and a constant sea ice thickness $h_i = 1\,\text{m}$. The sea ice velocity, $\boldsymbol{u_i}(= [u_i, v_i]^T)$ is a velocity vector of a point particle which makes d/dt as the total derivative. Here, u_i is the west-east/longitudinal or zonal velocity and v_i is the south-north/latitudinal or meridional velocity. Each of the beacon trajectories can then be simulated in time, based on point particles for each beacon, which are released at the start of the beacon trajectories at $t = 0$.

The shear stress terms based on a quadratic drag law McPhee (1982); Brown (1981) are given by:

$$\boldsymbol{\tau_{ai}} = \rho_a C_a (\boldsymbol{u_a} - \boldsymbol{u_i})|\boldsymbol{u_a} - \boldsymbol{u_i}|, \tag{3}$$

$$\boldsymbol{\tau_{wi}} = \rho_w C_w (\boldsymbol{u_w} - \boldsymbol{u_i})|(\boldsymbol{u_w} - \boldsymbol{u_i})|, \tag{4}$$

where ρ_a (1.2 kg/m^3) and ρ_w (1024 kg/m^3) are densities of air and water respectively, $\boldsymbol{u_a}$ is the surface air velocity, $\boldsymbol{u_w}$ is the surface water velocity, $C_a (= 1.2 \times 10^{-3})$ and $C_w (= 5.5 \times 10^{-3})$ are the coefficients of drag between the air-ice and water-ice interface whose values are obtained from McPhee (1982) and Brown (1981) and assumed to be constant. Wind drag is a term used interchangeably to refer to air-ice drag in this paper.

The point ice model represented by Eq. 2 is an Ordinary Differential Equation (ODE) with a time dependent non-linear inhomogeneous term. To evaluate the inhomogenous component in the model, we would need the wind and water velocities as well as the sea surface heights at each time instant. Now, this model is a simple, *standalone* sea ice model implying there is no coupling to any tidal, atmospheric or ocean circulation model. So, the simplification is that the required water levels, water velocities and wind data are obtained from existing and validated models or published datasets. These are then interpolated in space and time to the observed positions of the beacons at the respective time. This gives us a time series for wind and water velocities and gradients of sea surface heights with the values at each time being essentially the value from the corresponding dataset/model at the beacon position for the time. This serves a two-fold purpose, first by giving the point ice model the required data to compute the shear stress' and sea level gradient forcing in the model. And second, that interpolating the data to real-time beacon positions can be thought of as a one-way coupling or feedback between the point ice model and the other models.

Once these datasets are obtained, our point ice model is discretized using a Runge-Kutta 2 method with a constant time step of 30 s. The model then simulates only the ice velocities based on the forcing as per Eq. 2 where the external forcing are based on actual beacon positions.

3.3 External datasets/models

Three datasets (Table 1) are used to obtain the water levels, water velocities and wind data. The wind velocities are obtained from the

ERA5 hourly reanalysis product (Hersbach et al. 2018), while, for the water velocities we need two different dataset as the beacons are forced by both the ocean general circulation currents (ocean currents) and the tidal currents. Hence, the water velocity ($\boldsymbol{u_w}$) is obtained as a linear combination of both, i.e. $\boldsymbol{u_w} = \boldsymbol{u_{wo}} + \boldsymbol{u_{wt}}$, where $\boldsymbol{u_{wo}}$ is the ocean currents component in water velocity and $\boldsymbol{u_{wt}}$ is tidal currents component in water velocity. Similarly, the sea surface gradients are computed as the sum of the gradients from the sea surface heights obtained from the ocean general circulation model and tidal model ($\nabla\zeta_o + \nabla\zeta_t$, where the subscripts o and t denote ocean and tide respectively). The ocean circulation data are obtained from a global ocean analysis forecast product of CMEMS (Copernicus Marine Service 2014) and the tidal data is obtained from the GTSM Verlaan et al. (2015); Muis et al. (2016). After obtaining the data from the datasets, they are processed to derive the respective time series for each beacon needed to run the point ice model. The time series for velocities follow from the space-time linear interpolation. For the pressure gradient computation, spatial interpolations used a cubic 4 point interpolation and temporal interpolations were linear. The spatial gradients were computed using finite differences over a distance of 2.5 km. The grid step for the gradient computation is large compared to the beacon movement in the small model time step (30 s). The 30 s time step for the point ice model is only needed for stability of the explicit scheme and can likely be increased for an implicit scheme. The main time scale here, is tidal and on these time scales, grid step of 2.5 km is enough as tides do not change significantly over very short distances in open water.

3.4 Model validation

The point model simulated beacon velocities are obtained with the initial condition for the model runs given by the observed initial velocity. These simulated velocities are compared to the observed velocities for all the beacons. Here, we show comparison for beacon 16 (Fig. 4) where it is seen that the modelled time series' are very similar to the observed, especially in the initial part, for both, the longitudinal u_i and latitudinal v_i velocity. But, in time as the errors accumulate the differences increase between the modelled and observed values. Also, both, u_i and v_i velocities, have similar order of magnitude in modelled and observed values. The plots for remaining beacons show a similar behaviour (see Online Resource 1).

In the next test, we integrated the modelled velocities to obtain the simulated beacon positions and compared those to the observed ones. The velocity integration started with initial beacon position being obtained from the beacon observations. In general, we observe differences (Fig. 5) in the model-simulated beacon trajectories and corresponding observed trajectories for all the 6 beacons. But, the generic shape of the trajectories is captured fairly well. Particularly, the modelled beacon 14 (Fig. 5e) seems to have almost the same trajectory as observed. Beacons 03 and 16 (Fig. 5d, f) have the longest trajectories

Table 1 Description of the operational or published datasets for wind, ocean and tides and the corresponding variables used to build the point model

Type	Dataset	Grid Resolution	Time Res.	Variables	Time Span (2014)
Winds	ERA5 hourly reanalysis (Hersbach et al. 2018).	0.25 ° × 0.25 °	hourly	u10, v10 (10 m wind)	March 1 to May 16
Ocean	GLOBAL OCEAN ANALYSIS FORECAST E.U. Copernicus Marine Service (2014)	1/12 °	hourly	u, v, ssh at 0.45 m depth	March 15 to May 16
Tides	Global Tide and Surge Model v3.0 Verlaan et al. (2015); Muis et al. (2016)	5 to 25 km	15mins	u, v, ssh	March 15 to May 16

and their overall trajectories appear to be rotated clockwise (or towards west) in the simulations compared to the observations. Similar rotations are observed for trajectories of beacons 09 and 13 (Fig. 5c, d). The largest differences are seen for the simulated trajectory of beacon 02 (Fig. 5a). Further, it is noteworthy that in the plot we can only see differences in locations of the beacons but there may be differences in time as well. Another noteworthy aspect is that the modelled trajectories of beacons 03 and 09 (Fig. 5b and c) tend to go over the land boundary. This can be attributed to the fact that forward integration is used in our model and thus, it would not know about the presence of land bodies while computing the trajectory.

These discrepancies noted in the trajectories could have numerous reasons. First and foremost, the forward integration accumulates the velocity errors. Second, the model parameters (ice thickness and drag coefficients) are assumed to be constant, whereas in reality they could vary. Third, this point model is forced using output from external ocean, tidal and atmospheric models. Thus, there is no feedback from the ice solution on the ocean or tidal solutions. This could lead to artificial sea ice tidal response (Hibler et al. 2006). But using in-situ beacon positions, gives a priori knowledge of the ice response and hence, this factor can be alleviated to some extent. Additionally, the uncertainties or errors in the ocean, tidal and atmospheric models can also propagate in the point model simulations. Finally, the observed trajectories seem to move faster south of 76 ° latitude. This can be caused by the errors in ocean currents or winds, but also by the model itself. This is especially noticeable for the worse performing beacon 02 (Fig. 5a).

Nonetheless, our study focuses on the subdaily motion and the above observed discrepancies in trajectories should not be of major concern if the subdaily motion is correctly modelled. As seen from the plots (Fig. 5), not only the shape of the trajectories but also the clockwise loops (sea ice oscillations) are captured in simulations. An analysis of these subdaily loops of the simulations will shed light on the validity of our model.

The sea ice motion, as also seen in beacon trajectories, is made up of subdaily oscillations superposed with daily mean drift. The equation for this is given by:

$$u_i = u_{it} + u_{io}, \tag{5}$$

where u_i is the sea ice velocity vector or, in this case, the beacon velocities, u_{it} represents the subdaily oscillations (high-frequency) in the sea ice velocity and u_{io} is the mean drift (low-frequency) in the sea ice velocity.

To isolate the subdaily oscillations from the beacon trajectories, we apply a high-pass filter with a cutoff frequency corresponding to a period of 24 h. The resulting filtered signal is then, $u_{it} = [\delta u, \delta v]^T$, where west-east/longitudinal (δu) and south-north/latitudinal (δv) velocity time series are the subdaily oscillations in respective directions. To perform a quantitative examination of these oscillatory velocities, we do a discrete Fourier transform of the time series. The resulting amplitude and phase spectra are plotted and compared (Fig. 6) for modelled and observed oscillations along with the M_2, S_2, MU_2, and M_4) tidal and Coriolis/inertial frequencies (corresponding to 74.7 °N and 79 °N latitude).

First and most important aspect from the spectra is that the maximum amplitude for all the beacons occurs at a frequency which is close to the semi-diurnal tidal and inertial frequencies corresponding to 74.7 °-79 °N latitudes. Thus, one can say that the observed beacon oscillations in this region of the Barents Sea are clearly from the tides and inertial forces as was also noted previously in Section 2. But the magnitudes of these observed maximum amplitudes vary for each beacon with some having low amplitudes of around 0.1 m/s (Figs. 6a,b,g,h,e,f) to some having amplitudes of around 0.25 m/s (Figs. 6i,j,k,l). Furthermore, since the frequency resolution in the Fourier transform depends upon the length of the time series, we see multiple frequencies in between two consecutive frequencies on the spectrum for some beacons. For example, in the case of the shortest trajectory, beacon 14, M_2, S_2, MU_2 and both the Coriolis frequencies, all lie near the dominant frequency band and the next closest frequencies are far apart. Consequently, the amplitudes and phases at such points in the spectrum have an influence of all the frequencies falling in their band. Additionally, it should be noted that this Fourier transform approach averages the changes in the oscillations over the entire time series which implies that the obtained/plotted amplitudes and phases here are time averages of the beacon trajectory.

Comparing the observed and modelled Fourier transforms, it can be seen that both the spectra have similar order of magnitudes of the amplitudes and phases at the tidal and inertial frequencies for all the beacons. For frequencies with low
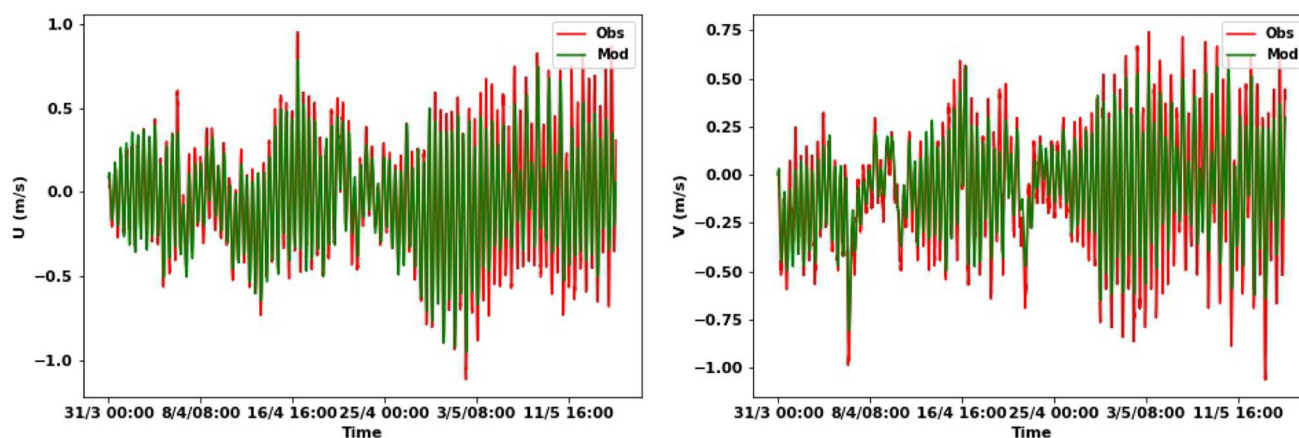
Fig. 4 Time series plot for the longitudinal (u_i) (U in plot) and latitudinal (v_i) (V in plot) velocities for beacon 16. Observations are in red and point model simulations are in green. Time on the x–axis is given in format DD/M HH:MM with year being 2014. The velocities are plotted at the same time of the observations of the beacon positions, and thus, are separated by a time step of 15 min

amplitudes, the phase, naturally, becomes very uncertain which is probably the reason for the noisy phases in the spectra.

Of the semi-diurnal frequencies, it is seen that the maximum amplitude in both the observed and modelled spectra occurs at M_2 frequency. But the magnitudes of the modelled amplitudes for the dominant M_2 frequency are consistently lower than the observed amplitudes. In a more quantitative sense, the modelled amplitude at M_2 frequency for δu and δv velocity oscillations are anywhere between $70 - 90\%$ of the observed values for all the beacons. Thus, based on the above qualitative comparison coupled with a good accuracy at the dominant M_2 frequency one can say that our 'simple' point model reasonably captures the amplitude and phase spectra as compared to the observed spectra. As such, our model is suitable to perform further analysis on the subdaily sea ice oscillations even if it does not reproduce the trajectories accurately. Next, we will evaluate the dissipation between the sea ice-tide interface by performing two analyses which study the correlation and causality of sea ice oscillations.

4 Correlation between sea ice oscillations and tides

4.1 Aim and methodology

The aim is to investigate the relationship between tidal currents and the sea ice oscillations by comparing the observed oscillations to the point model oscillations and the tidal currents from the GTSM in the Barents Sea region.

For this analysis, we use the subdaily sea ice velocity signals (δu and δv) of point model simulations and observations obtained previously (Section 3) by high-pass filtering the beacon velocities. To compute the tides, the GTSM was run without any atmospheric forcing and as mentioned before,

it does not include the effect of sea ice on tides. Thus, the tides can be considered independent of the wind and sea ice effects. To study the relationship, the velocity vectors of the subdaily oscillations (modelled and observed) and tidal velocity vectors are plotted on a time axis. The relationship is further quantified by computing the corresponding correlation coefficients.

4.2 Results and discussion

For each beacon, we have two plots, the vectors of beacon observations versus tidal velocity vectors and another, vectors of beacon observations versus vectors of point model simulations. The plots for beacon 16 (Figs. 7 and 8) are presented and discussed here.

It can be seen that all the velocity vectors loop clockwise along the time axis. This resembles the loops formed by an elongated spring where the loops have different radii corresponding to the magnitude of the vectors. One can view these plots as tidal ellipses stretched over time, but, since the beacon moves over time the shape of the ellipse depends on the tidal currents at the beacon location. On comparing the loops of the tidal velocity vectors or tides against the observations in Fig. 7, it is seen that, in general, the highs and lows of the oscillations (vector magnitudes) occur at almost the same times and the loop inclinations (vector directions) are also, almost, the same throughout the length of the series. In the initial period, the tidal vectors and observed oscillations are seen to have a better match in terms of the magnitude and direction of the vectors. And, towards the end, the observations have a larger magnitude than the tides and their directions seem rotated. The larger amplitudes of the observed oscillations towards the end for this beacon is also evident from the larger loops/tidal ellipses in its trajectory (Fig. 5f) in the region around Bear Island. The tidal

(a) 02

(b) 03

(c) 09

(d) 13

(e) 14

(f) 16
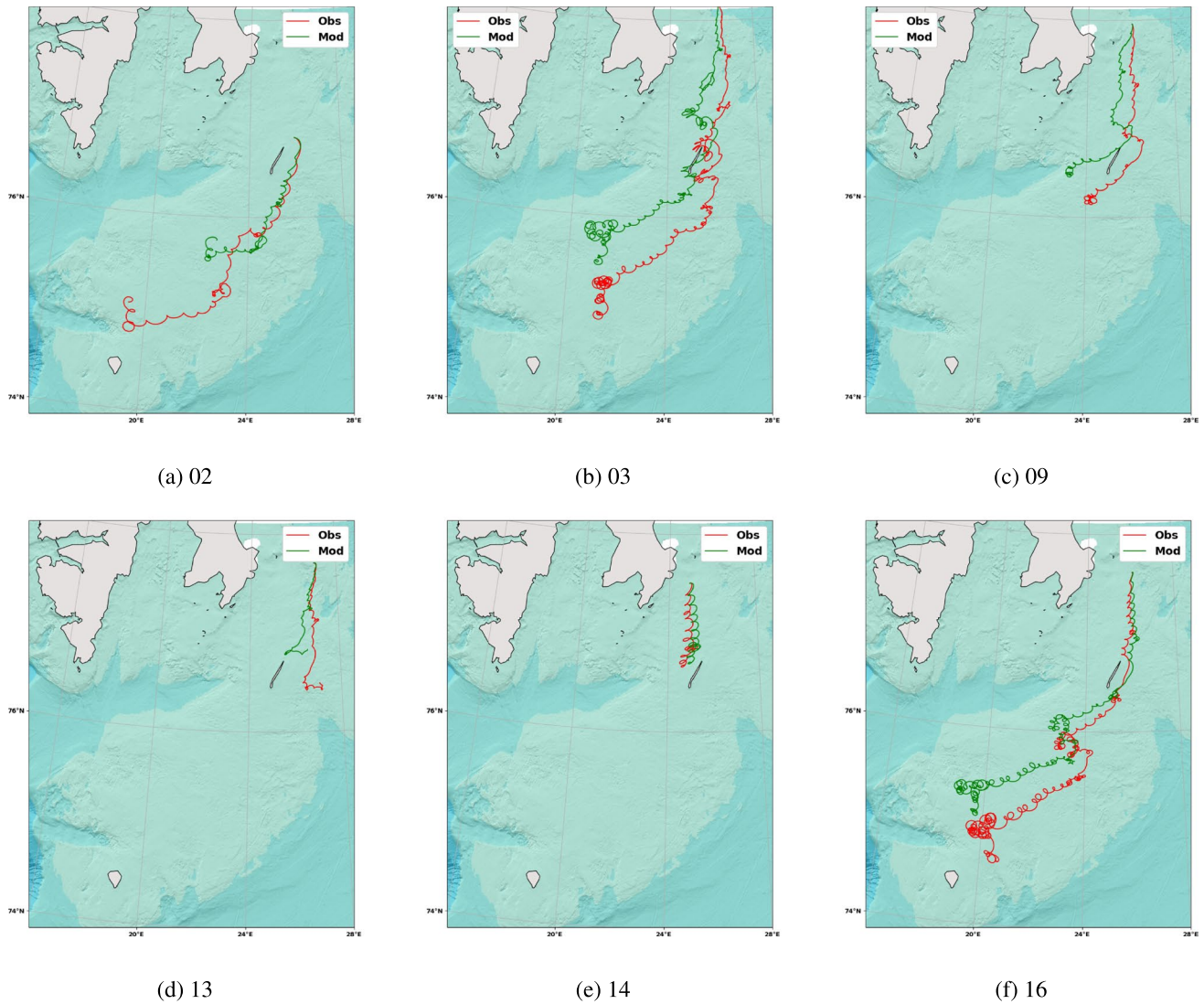
Fig. 5 Modelled drift trajectories for the beacons against the observed trajectories. The caption under each figure gives the beacon number. All the modelled trajectories are computed using a constant ice thickness of 1.0 m. The start date and time for all the simulations is chosen as March 31, 00:00 am because post this all the beacon trajectories are below 78 °N latitude

currents (Fig. 2) are also stronger in this region which hints to a correlation between the two. Another interesting part is when the tides seem to have died out or tidal velocity vectors have low amplitudes (Fig. 7; time period April 7 to April 12) the corresponding observations are also very low, and, are almost of the same magnitude. Thus, it can be concluded that the observed oscillations and tidal velocity vectors have similar highs and lows along the entire time series.

Such a similar behaviour is also observed in the case of comparison between observed and modelled oscillations (Fig. 8) with a difference only in the initial part of the trajectory where the point model oscillations are smaller (vector magnitudes lower) and the oscillations tilted to right (vectors are rotated clockwise). It implies that the point model captures the subdaily oscillations fairly well and is

an additional validation of the point model results. For other beacons (plots shown in Online Resource 2), similar conclusions can be drawn.

To further quantify the agreement between the observed oscillations on the one hand and the tidal velocity vectors and the point model oscillations on the other hand, correlation coefficients were computed for the δu and δv velocities (Table 2). This is done for each of the 6 beacons.
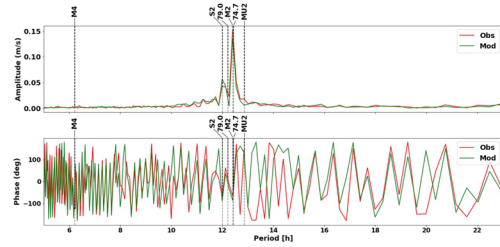
The values in both the cases are positive and large (> 0.8, for all beacons) suggesting a direct and strong relationship between the tides and sea ice oscillations. This in turn implies that the sea ice oscillations and the corresponding tidal currents move together in Barents Sea region. Moreover, it implies that the sea ice oscillations have a dominant
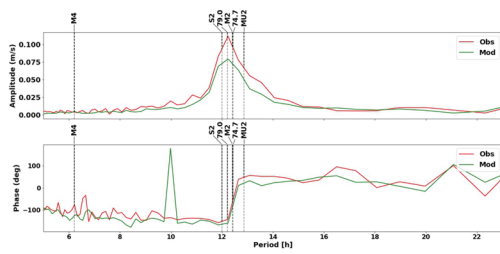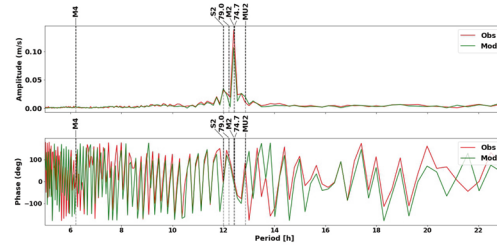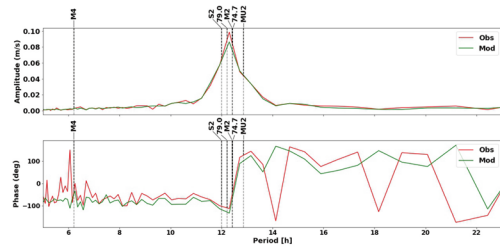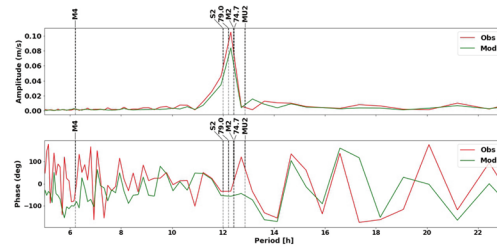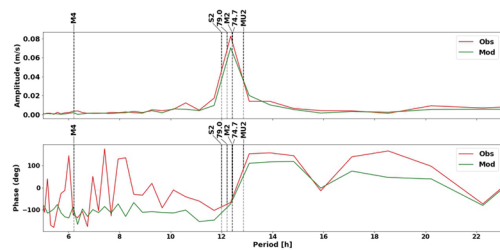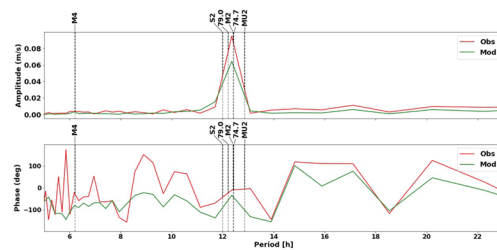
(a) 02:U
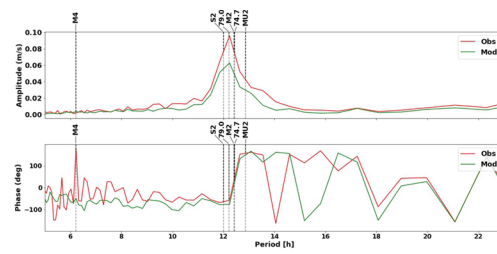
(b) 02:V

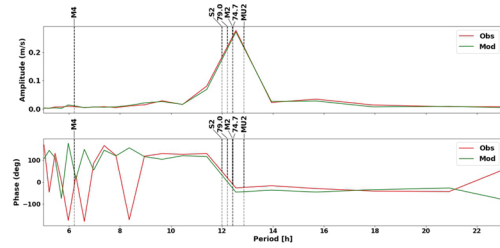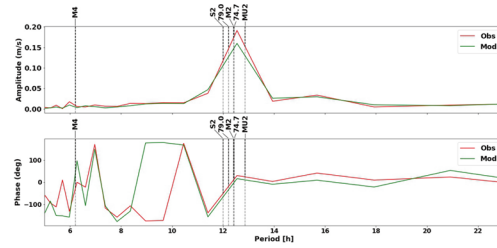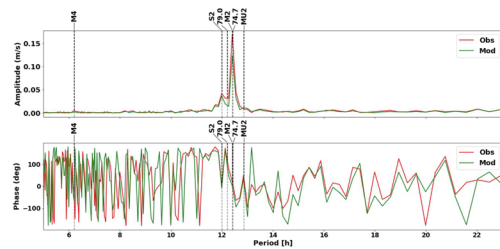(c) 03:U

(d) 03:V

(e) 09:U

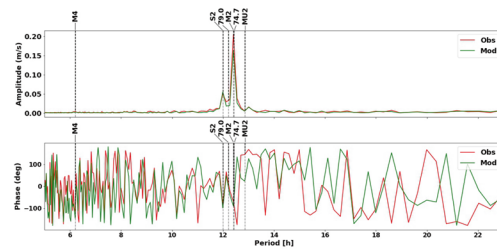(f) 09:V

(g) 13:U

(h) 13:V

(i) 14:U

(j) 14:V

(k) 16:U

(l) 16:V

◄**Fig. 6** Amplitude and phase plots of the velocities from beacon observations (red) and point model simulations (green) against time periods in the oscillations. The periods are in subdaily range (i.e. high frequency) from 5 h to 23 h. Apart from the inertial and tidal frequencies denoted by dotted lines, the remaining high frequency spectra are red noise. The subfigure captions denote the beacon number and the U and V correspond to δu or δv velocity respectively

tidal signal as opposed to an inertial signal, a conclusion in line with Pease et al. (1995).

The correlation between observed and point model oscillations is similar to the observed oscillations and tidal vectors. This means that the forcing responsible for tides in GTSM and point model are similar suggesting that the tidal forcing could be a major cause of sea ice oscillations in this dataset. Next section will verify this with a sensitivity analysis.

5 Causality of sea ice oscillations

5.1 Aim

We have shown a strong and positive correlation between sea ice oscillations and tides/tidal currents. However, *correlation does not imply causality*. The cause of the sea ice oscillations is still unknown. There are many possible forcing which could cause the subdaily sea ice oscillations like, inertia or Coriolis forcing, wind drag (air-ice drag), pressure gradients from the sea surface heights associated with tides or the water-ice drag from tidal currents. Here, we aim to study the cause of the sea ice oscillations. When coupled with the previous analysis this will help to determine the energy dissipation between the sea ice-tide interface. We start by establishing an hypothesis, formed by performing a preliminary analysis of the dynamics between sea ice and tides followed by sensitivity tests to verify the hypothesis.

5.2 Preliminary analysis of the dynamics

From the results shown in Section 4, we hypothesize that tidal forcing is the major cause of sea ice oscillations. Moreover, from the equations of point model or free drift model (Eq. 2) it is clear that this forcing comprises of the pressure gradients from the tidal sea surface heights and water-ice tidal drag. One can argue that, in practice, these two are always present together, yet it is important to evaluate which of the two is the primary cause of the sea ice oscillations.

If it is pressure gradient forcing then it follows that the tidal model and sea ice model are forced by the same forcing and the bottom frictional stress from the shallow water region or the viscous term does not play a significant role. In such a case, the water-ice drag term is comparatively low and the connection between sea ice and tide is not strong, consequently, giving us a negligible dissipation from drag in the sea ice and tide interface. On the other hand, if water-ice drag term is the primary cause of the sea ice oscillations then the stress from this term is significant and the connection between sea ice and water is strong. This would further mean that the dissipation between the ice-tide interface needs to be evaluated to ascertain the nature.

To evaluate a priori which of the above two forcings might be a cause, we conduct a scaling analysis on Eq. 2.

Consider U, H and T as scaling factors for the velocity, ice thickness and time, respectively. Then the subdaily (or tidal scale) ice velocity can be written as $\boldsymbol{u_{it}} = U\boldsymbol{u_{it}^*}$. Similarly, the remaining terms in the ice-drift Eq. 2 are written as $t = Tt^*$, $h_i = Hh_i^*$, $\boldsymbol{u_{wt}} = U\boldsymbol{u_{wt}^*}$.

Now, assuming that the water-ice drag from tides is a major significant force we have the local/inertial acceleration term equated with this drag which is further scaled with $\rho_w C_w U^2$ (water-ice tidal drag). Thus, the equation looks like,

$$\rho_i h_i \frac{\partial \boldsymbol{u_{it}}}{\partial t} = \boldsymbol{\tau_{wi}},$$
$$\Rightarrow \frac{\rho_i H U}{T} \frac{\partial \boldsymbol{u_{it}^*}}{\partial t^*} = \rho_w C_w U^2 (\boldsymbol{u_{it}} * -\boldsymbol{u_{wt}^*})^2, \quad (6)$$
$$\Rightarrow \frac{\rho_i H}{\rho_w C_w UT} \frac{\partial \boldsymbol{u_{it}^*}}{\partial t^*} = (\boldsymbol{u_{it}} * -\boldsymbol{u_{wt}^*})^2.$$

The factor $\frac{\rho_i H}{\rho_w C_w UT}$ is the Strouhal's number (Sr). As we know that M_2 is the dominant frequency in the sea ice oscillations in the Barents Sea and also, it is very close to the inertial frequencies in the region, consider T as $T_{M_2}(\sim 4.4 \times 10^4 \text{ s})$. Also, assuming $H = 1$ m and $U = 0.1$ m/s the value of $Sr \sim 3 \times 10^{-2}$. Thus, $Sr << 1$ which implies $\boldsymbol{u_{it}^*} \approx \boldsymbol{u_{wt}^*}$ as per Eq. 6. Thus, the sea ice oscillations and tidal velocities/tidal currents must be similar. As a result, the sea ice will be dragged along with the tides attaining almost the same velocity as tides. This would mean that the nonlinear connection between sea ice and water is strong and the water-ice tidal drag is large and a possible major cause of sea ice oscillations.

One can also calculate the time-scale for which the terms become of comparable magnitude, i.e. $Sr \sim 1$. Consequently, $T \sim 1.6 \times 10^3$ s or approximately 0.5 h is the actual inertial timescale of sea ice drift. Thus, on an M_2 tidal time scale, the sea ice attains a steady state equilibrium condition. Such a timescale of $T \sim 10^3$ s is also shown in Leppäranta and Leppäranta (2011a).

As most of the sea ice is in steady state equilibrium on M_2 tidal time scale, we study the case of steady state ice drift equation but with only the pressure gradients from tidal sea surface heights to understand the significance of the forcing. The Eq. 2 then, reduces to:
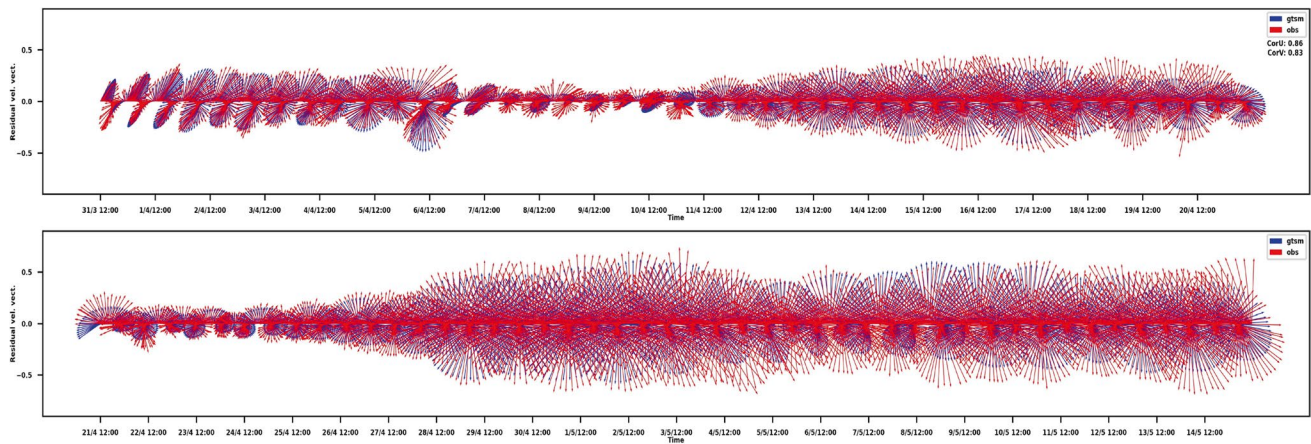
Fig. 7 Velocity vector plots of the time series of sea ice oscillations (δu and δv) with observations (red) and GTSM tides (blue) for beacon 16. The residual velocity vectors imply that the mean drift is removed from the beacon trajectories and the resulting subdaily residuals are plotted
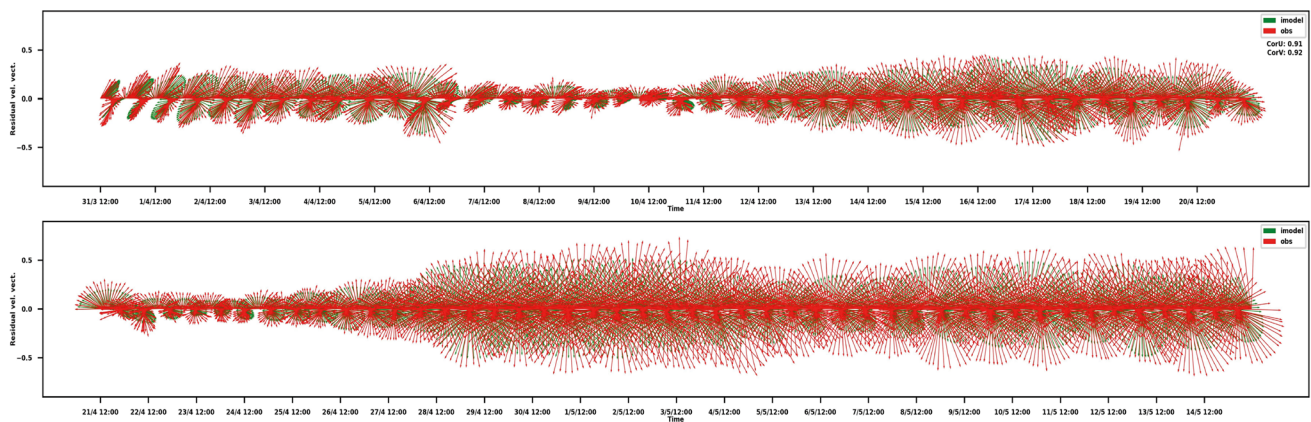
Fig. 8 Velocity vector plots of the time series of sea ice oscillations (δu and δv) with observations (red) and point model oscillations (green) for beacon 16. The residual velocity vectors imply that the mean drift is removed from the beacon trajectories and the resulting subdaily residuals are plotted

$$fe^{i\pi/2}\boldsymbol{u}_g = -g\boldsymbol{\nabla}\zeta_t. \tag{7}$$

This is a form of the geostrophic flow equation, where $\boldsymbol{u}_g$ is the steady state ice velocity originating only from the pressure gradient of tidal sea surface heights. The velocities are computed using the above equation for all the beacon trajectories. Then the mean of the magnitude of the resulting velocities ($\overline{|\boldsymbol{u}_g|}$) along the beacon trajectories is compared to the mean of the magnitude of tidal velocities ($\overline{|\boldsymbol{u}_t|}$) along the

beacon trajectories. Then, it evaluates that, for all the beacons, $\overline{|\boldsymbol{u}_g|} \sim 20\%$ of $\overline{|\boldsymbol{u}_t|}$. Now, from the analysis present in Section 4, we know that the tidal velocities and subdaily sea ice velocities are very close. As a result, it can be said that forcing from pressure gradients of tidal sea surface heights might contribute around 20% to the sea ice oscillations. Hence, this forcing, although a cause of sea ice oscillations, is probably not a dominant one for this Barents Sea dataset.

Table 2 Correlation between beacon observed sea ice oscillations, GTSM derived tidal currents and point ice model based sea ice oscillations. The U and V represent the δu and δv velocity of the oscillations, respectively

	02		03		09		13		14		16	
	U	V	U	V	U	V	U	V	U	V	U	V
Tides-Obs	0.89	0.82	0.82	0.80	0.90	0.83	0.91	0.82	0.93	0.90	0.86	0.83
Mod-Obs	0.91	0.92	0.86	0.89	0.93	0.89	0.92	0.86	0.94	0.95	0.91	0.92

Based on the above mathematical analyses we hypothesise that the water-ice tidal drag is the major reason behind the sea ice oscillations in this Barents Sea dataset.

5.3 Sensitivity analysis on the forcing

To evaluate the hypothesis and strengthen our understanding, we perform a number of sensitivity tests on the beacon dataset for all the forcing and not only the tidal forcing. These tests are done on the parameters of the sea ice model Eq. 2. In this analysis, the effects of different model and forcing parameters on the sea ice oscillations are assessed by switching the respective parameter or forcing off and running the model. The resulting model runs are compared to the *reference* model runs and the observations. Reference model here is defined as the model where all the forcing from the Eq. 2 are included and the model results are the ones discussed in Section 3. Such a comparison provides the magnitude of the effect that respective forcing has on the sea ice oscillations.

As observed previously (Fig. 6), M_2 frequency is the dominant one in the observed oscillation spectrum and this is also very close to the inertial frequencies. Because of this dominance, the sea ice can be considered to be majorly oscillating at this frequency. Hence, we use the amplitude and phase at a frequency which falls close to the M_2 frequency in the observed and modelled spectra of oscillations as a comparison metric. And furthermore, the oscillations at this frequency will be referred to as M_2 *frequency oscillations*. Thus, for comparison the amplitude and phase of the M_2 frequency sea ice oscillations (δu_i and δv_i) are obtained from the reference model runs and model runs without a particular forcing parameter from Table 3.

For the sea ice inertia (Table 3), the test involves performing model runs for varying sea ice thicknesses from 0.5 m to 3.0 m. Here it should be noted that the reference model thickness was 1.0 m. In the case of wind drag forcing, the test involves running the model by just switching off the winds ($\boldsymbol{u_a}$).

The last of the sensitivity analyses is based on tidal forcing where two tests were performed, one without pressure gradients from tidal sea surface heights (tidal pressure gradient forcing) and one without the tides/tidal currents in the water-ice drag. Note that removing the tides in water-ice drag is equivalent to not considering water-ice tidal drag when we are evaluating M_2 frequency oscillations.

The sensitivity analysis for ocean currents and their corresponding pressure gradients is not conducted because they have no tides in them and thus, they will not cause M_2 frequency oscillations.

5.3.1 Effect of ice thickness

The results (Fig. 9) shows that for all thicknesses and all beacons, observations have a larger amplitude and their phase is lagging for both the δu and δv velocity compared to model runs. The values of the amplitudes of the δu and δv velocity beacon observations vary from 0.1 m/s to around 0.25 m/s which is in line with the values noted in Section 3.

There are small variations in the amplitudes of the δu and δv velocity components in the model runs with varying sea ice thicknesses for all the beacons. These variations depend on the magnitude of the amplitude. For instance, amplitudes of beacons 03, 14 and 16 are larger than the other three beacons and thus, the variations in the modelled amplitudes are also larger. The corresponding phases also seem to vary, but much less than the amplitudes. These minor variations in the amplitudes and phases are probably a numerical artefact. Hence, they can be ignored and it can be said that the sensitivity analysis shows no effect of sea ice thickness on the amplitude and phase of M_2 frequency oscillations for a broad range of sea ice thicknesses for the beacon dataset. This is in line with Omstedt (1980), who found using a sensitivity analysis of steady-state free drift sea ice motion that sea ice mass has no significant effect on free drift of sea ice.

The lack of any significant effect can also be seen from a dimensional analysis as presented in Section 5.2 where we evaluated based on Strouhal's number that the sea ice inertial timescale is $T \sim 0.5$ h. Now, time scale of M_2 tide is $T_{M_2} \sim 12.42$ h. Consequently, for sea ice thickness to have any significant effect on the oscillations at M_2 frequency it should have a thickness of around 20 m for $U = 0.1$ m/s (i.e., $T \sim 12.42$ h). This is unrealistic.

However, note that the results in Fig. 9 are valid only when the model assumes a free drift sea ice. This is because even for the case of 2 or 3 m thick ice (Fig. 9) the sea ice internal stresses start to play a role and its effect on sea ice oscillations might be different.

5.3.2 Effect of wind drag forcing

The results of these model runs (Fig. 10) show that the observations are larger in amplitudes and lagging in phase compared to the reference model.

The δu amplitudes of model runs without the wind drag forcing are around $2 - 4\%$ higher than the reference model runs with the differences varying for all the beacons. These differences seem to scale with the initial magnitude of the reference model runs, cf. beacon 14 to beacon 13. Similar effect is observed for the δv amplitudes too. Thus, it can be

Table 3 Sensitivity tests conducted on the point model forcing and corresponding parameters. It should be noted that only the given parameters above are switched off in the respective tests, the remaining parameters are still present in the model simulations

| Forcing	Parameters
Sea ice inertia	h_i
Wind Drag forcing	$\boldsymbol{u_a}$
Tidal forcing	$\boldsymbol{u_t}; \boldsymbol{\nabla \zeta_t}$

said that the wind forcing tends to dampen the amplitudes of M_2 frequency oscillations of δu and δv velocity. Further, there is almost no change observed in the phases of both the δu and δv amplitudes by removing the wind drag in the model runs.

The results indicate that the wind drag forcing has a very small but noticeable influence on the δu and δv amplitudes of the sea ice oscillations (Fig. 10). The large effect observed for beacon 14 could be explained by the comparatively short lifespan of this beacon as a result of which the Fourier transform is not able to distinguish between M_2, S_2, and inertial frequencies. Consequently, their individual effects are superimposed on each other magnifying the effect of inertial forcing. This can also be seen in the Fourier transform of the oscillations of this beacon (Figs. 6i, j and 11).

The relatively small changes in the amplitude and phases due to wind drag forcing implies that the wind drag is not a major cause of the sea ice oscillations in our dataset. Thus, the inertial oscillations from this forcing are not dominant in the sea ice oscillation, which supports the conclusion of our first analysis (Section 4). This conclusion is in line with

the analysis of Pease et al. (1995) and Kowalik (1981), but in contradiction to Hibler et al. (2006).However, Hibler et al. (2006) model results were for the inertial wind forcing with sea ice drifting under strong internal stresses and their model domain was central Arctic and Siberian Continental Shelf.

In the free drift subdaily sea ice velocity spectrum where the external forcing (wind or tidal drag) is periodic, a peak is observed when the frequency of external forcing is equal to Coriolis frequency Leppäranta and Leppäranta (2011b); Omstedt et al. (1996). This peak is an analytical aspect from the nature of the free drift equation with a linear stress law used for the respective air-ice and water-ice drag terms. The analytical and model results are given in Omstedt et al. (1996). Now, as the Coriolis frequency is almost the same as semi-diurnal tidal frequencies in the Barents Sea region, the resulting sea ice velocity spectrum has a peak at semi-diurnal tidal frequencies. This is evident from the beacon observed spectrum (Fig. 6). So for inertial forcing to have a significant effect on the sea ice oscillations, they should posses strong semi-diurnal frequency signals. In the current beacon experiment, the winds did not possess strong

(a) U Amp

(b) U Ph

(c) V Amp

(d) V Ph
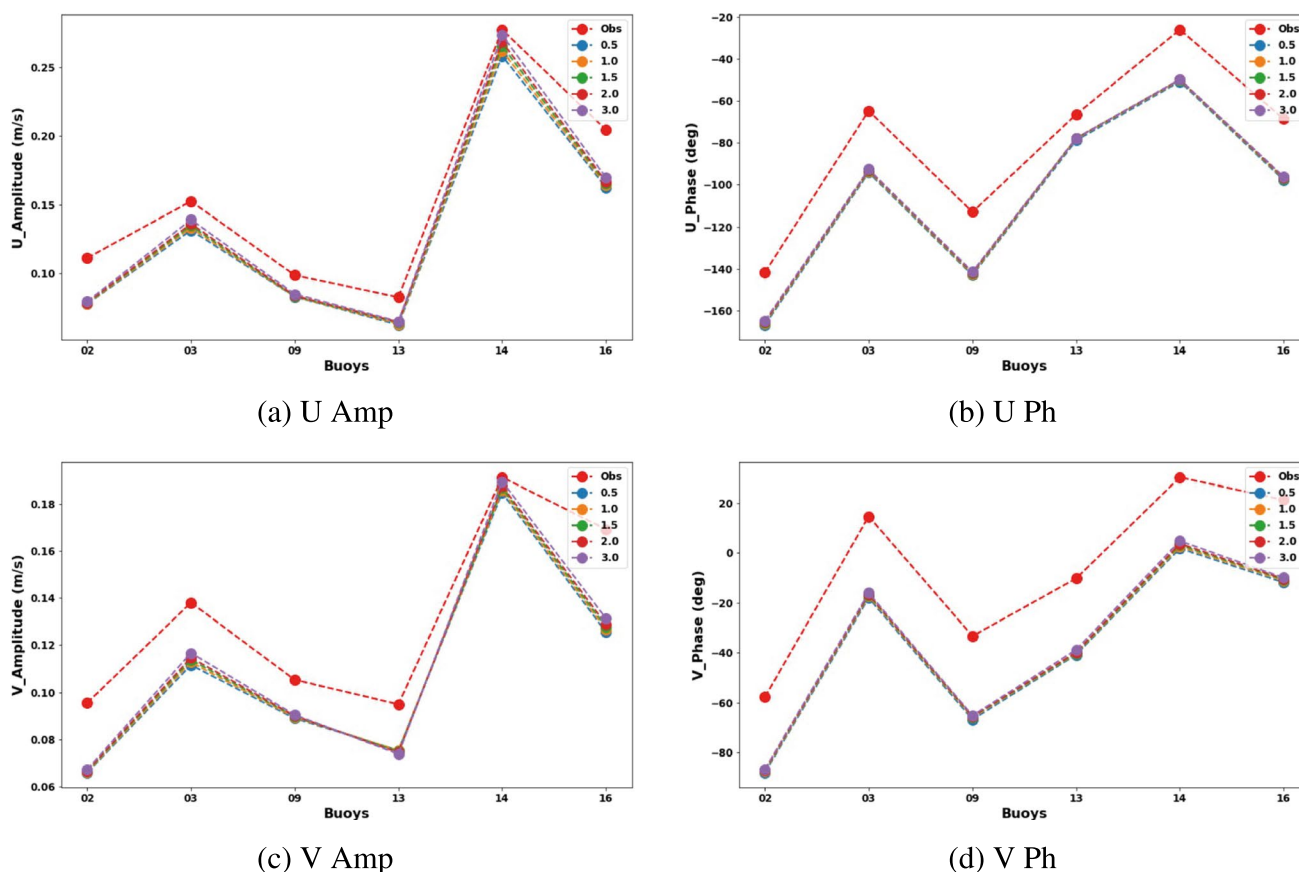
Fig. 9 Plots of M_2 amplitudes and phases ($y-$ axis of the δu and δv velocity components of the sea ice oscillations against the beacons on $x-$ axis. The beacon observations (red) are compared against the point model simulations with varying sea ice thicknesses. The M_2 frequency amplitude and phase are obtained from the Fourier transform plots (Fig. 6)

subdaily frequency signal and hence, its effect was low on sea ice oscillations. But in the case of storm surges, the winds might have stronger subdaily signals, which will have significant effect on the sea ice oscillations. One such example was noted in the strong cyclone-induced inertial sea ice oscillations in the Fram Strait (Lammert et al. 2009). Thus, we conclude that in the beacon dataset the wind drag is a cause of sea ice oscillations albeit not a dominant one. This is valid for the winds obtained from ERA5 (Hersbach et al. 2018). in which no strong subdaily scale signal was present.

5.3.3 Effect of tidal forcing

For the first test, the results indicate that for model runs without water-ice tidal drag, the amplitudes of the M_2 frequency oscillations of δu and δv velocity are very low (< 0.03 m/s). While for phases, it is seen that the δu velocity phases are lagging the reference model and δv velocity phases are leading the reference model. The amount of lead and lag in the phases is varying for each beacon but for such

low amplitudes one cannot make physical sense from the phases and hence, can be ignored.

On the other hand, for the test without pressure gradients from tidal sea surface heights (Fig. 12) there is a small reduction in δu and δv velocity amplitudes. It is seen that the reduction of δv velocity amplitudes is comparatively larger than for the δu velocity. Similarly, there is a small change of phase of a few degrees with the runs without pressure gradients leading the reference model runs. Beacon 14 again has a comparatively larger deviation in the amplitudes compared to reference model runs than other beacons. This is again attributed to the aspect of the combination of the nearby frequencies (M_2, S_2, and inertial frequencies) in the Fourier transform.

From the results, it can be inferred that removing the tidal currents significantly dampens the amplitudes for all the beacons consistently. Further, the relatively small changes of amplitudes upon removing the pressure gradients from tidal sea surface heights implies that their effect on sea ice oscillations is low. This is in line with our hypothesis and as also

(a) U Amp

(b) U Ph

(c) V Amp

(d) V Ph
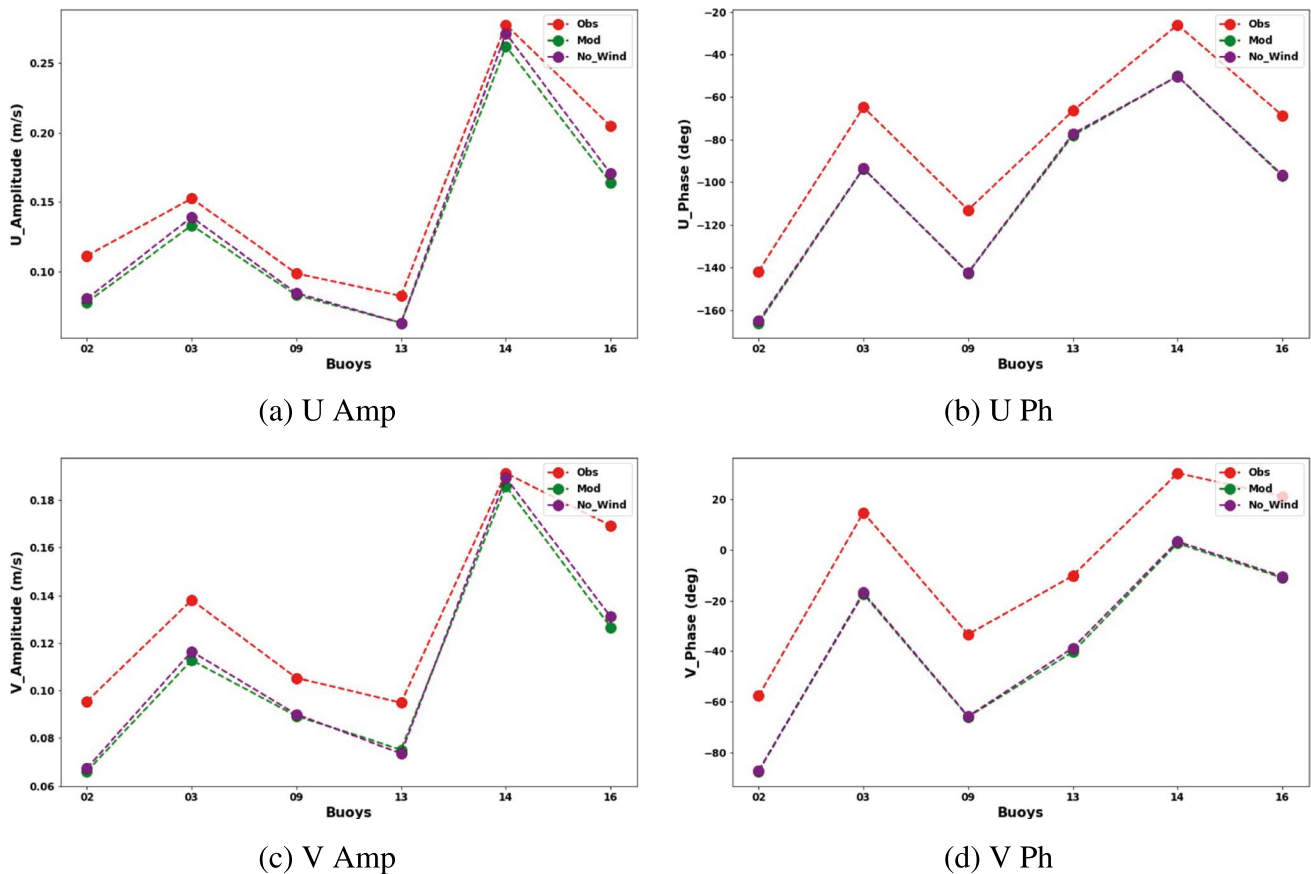
Fig. 10 Plots of M_2 amplitudes and phases of the δu and δv velocity components of the sea ice oscillations against the beacons on x−axis. The beacon observations (red) are compared against the point model simulations with and without wind (air-ice drag) forcing. The reference point model simulation (referred to as Mod in legend; green colour) is the model run with all the forcing as given by Eq. 2 and ice thickness of 1 m. The point model simulation without wind drag and coriolis force is the one labelled as *no wind drag forcing* (purple colour). The M_2 frequency amplitude and phase are obtained from the fourier transform plots (Fig. 6)

(a) U Amp

(b) U Ph

(c) V Amp

(d) V Ph
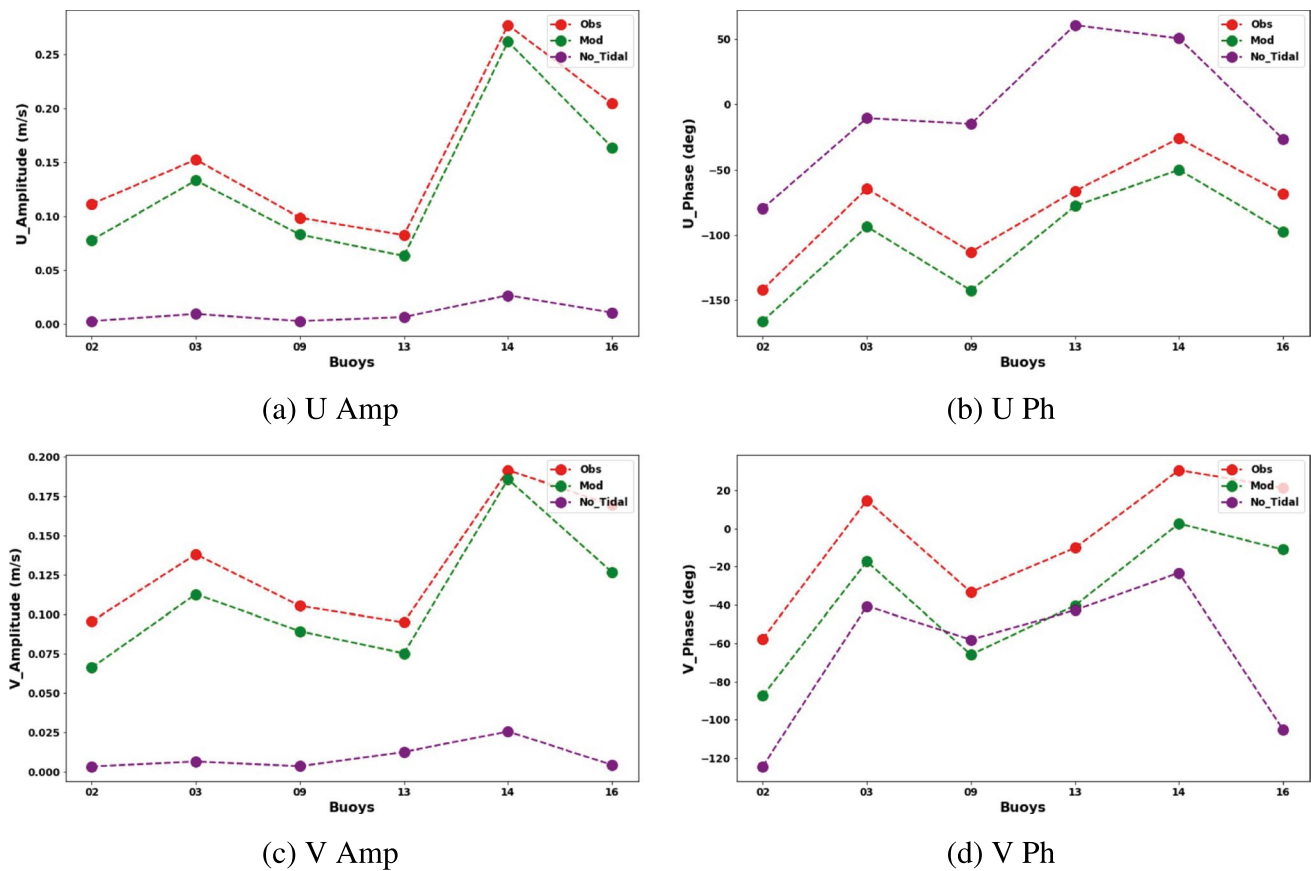
Fig. 11 Plots of M_2 amplitudes and phases of the δu and δv velocity components of the sea ice oscillations against the beacons on $x-$ axis. The beacon observations (red colour) are compared against the point model simulations with and without tidal currents. The reference point model simulation (referred to as Mod in legend; green colour) is the model run with all the forcing as given by Eq. 2 and ice thickness of 1 m. The point model simulation without any tidal currents is the one labelled as *No Tidal* (purple colour). The M_2 frequency amplitude and phase are obtained from the fourier transform plots (Fig. 6)

noted in Steele et al. (1997). Thus, the analysis shows that tidal currents and the resulting drag is essential and a major cause for the dominant M_2 frequency sea ice oscillations in the observations of the Barents Sea.

In this dataset of Barents Sea region there is a strong correlation between the sea ice oscillations and the underlying tides implying the relative velocity between the two is low. It is also seen that the water-ice tidal drag is the main cause of the sea ice oscillations. This makes the coupling between sea ice and tides strong and hence, the shear stress between the two is large.

## 6 Analysis on energy dissipation

The quantitative nature of the energy dissipation between the air-ice and water-ice interface on a subdaily scale for the Barents Sea experiment is not straightforward. In this section, we evaluate energy loss/transfer due to both the drags in their respective interface. For this, we use the point model derived

sea ice velocities to evaluate the energies since it is a validated for the subdaily oscillations and uses the free drift Eq. 2. Moreover, we use the tidal model dataset from GTSM that is based on Eq. 1. The comparison metric for the computed energies is the energy loss of tidal energy to the bottom/bed friction since this friction is the main source of tidal dissipation globally. The expression for this is given by:

$$E_b = -\boldsymbol{\tau_b} \cdot \boldsymbol{u_{wt}}, \tag{8}$$

$$E_b = -\rho_w C_b |\boldsymbol{u_{wt}}| \boldsymbol{u_{wt}} \cdot (\boldsymbol{u_{wt}}),$$
$$\overline{E_b} = -\rho_w C_b \overline{|\boldsymbol{u_{wt}}|^3}, \tag{9}$$

where E_b is the energy loss to bottom friction, $\boldsymbol{u_{wt}}$ is the tidal velocity along the beacon trajectory, $C_b (1.2 \times 10^{-3})$ is the bottom friction coefficient as used in the GTSM model runs. E_b is the energy loss over the entire trajectory of each beacon and it is different for each beacon. Hence, a time-average is computed over the M_2 period given by $\overline{E_b}$.

(a) U Amp

(b) U Ph

(c) V Amp

(d) V Ph
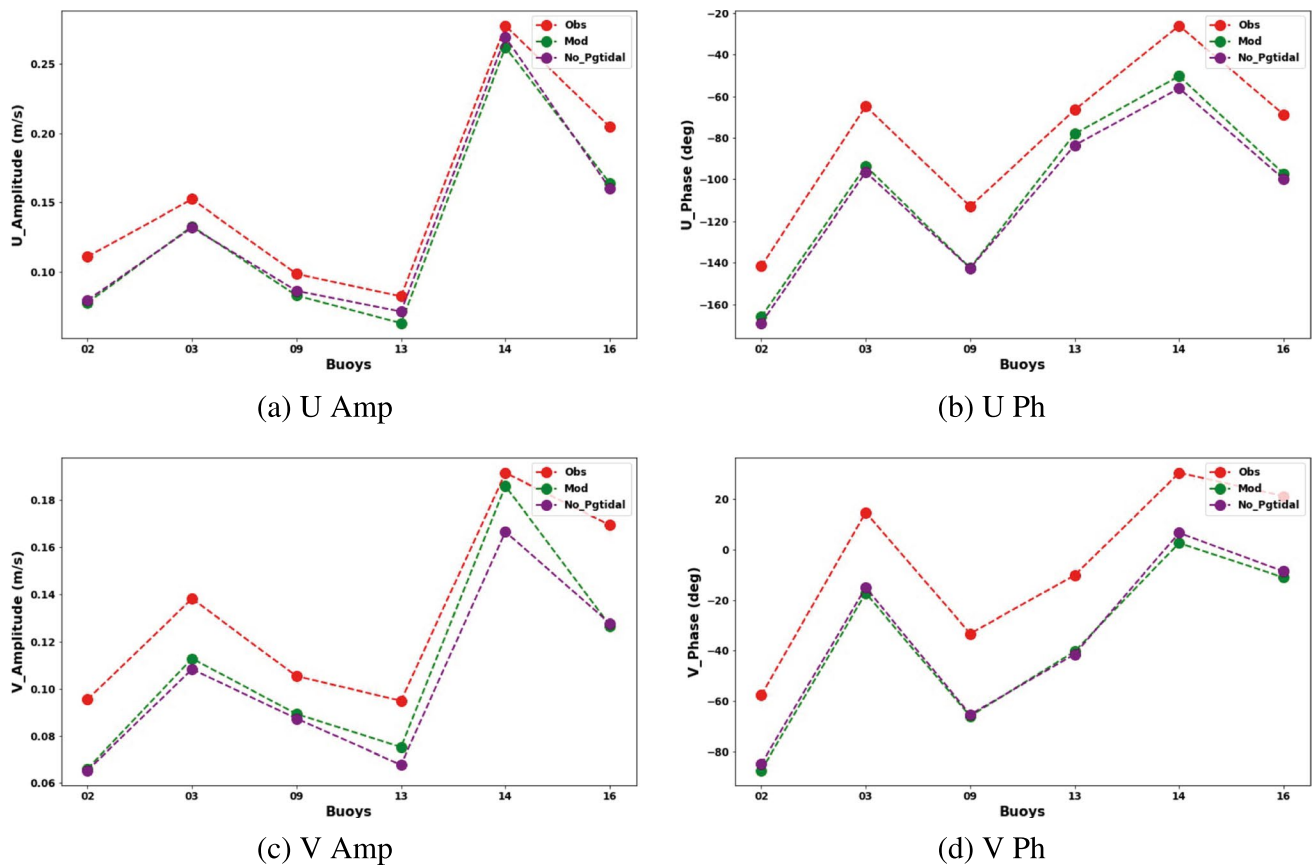
Fig. 12 Plots of M_2 amplitudes and phases of the δu and δv velocity components of the sea ice oscillations against the beacons on $x-$ axis. The beacon observations (red colour) are compared against the point model simulations with and without pressure gradients from tidal sea surface heights. The reference point model simulation (referred to as Mod in legend; green colour) is the model run with all the forcing as given by Eq. 2 and ice thickness of 1 m. The point model simulation without the pressure gradients from tidal sea surface heights is the one labelled as *No Pgtidal* (purple colour). The M_2 frequency amplitude and phase are obtained from the fourier transform plots (Fig. 6)

6.1 Dissipation from strong winds

It was seen previously that the wind drag plays a significant role in sea ice oscillations in the Barents Sea, only when there is strong subdaily signal in the winds. But this conclusion was motivated from the analysis of Omstedt et al. (1996) who assumed a linear drag law for air-ice drag. In practice, a quadratic drag law is used and this non-linear quadratic term in itself can have a dissipation part which might affect the subdaily sea ice oscillations.

The energy from wind drag (air-ice drag) on sea ice, is given by:

$$E_{ai} = \boldsymbol{\tau_{ai}} \cdot (\boldsymbol{u_i}), \tag{10}$$

where E_{ai} is the energy loss from the air-ice drag $\boldsymbol{\tau_{ai}}$. The remaining terms are same as in Eq. 3. Then, the dissipation component in this wind stress is seen by performing a linearisation of the stress by Taylor's approximation.

$$\boldsymbol{\tau_{ai}} = \rho_a C_a \sqrt{u_a^2 + v_a^2} \begin{bmatrix} u_a \\ v_a \end{bmatrix} - 2\rho_a C_a \sqrt{u_a^2 + v_a^2} \begin{bmatrix} \delta u_i \\ \delta v_i \end{bmatrix} +$$
$$\frac{\rho_a C_a (u_a \delta v_i - v_a \delta u_i)}{\sqrt{u_a^2 + v_a^2}} \begin{bmatrix} -v_a \\ u_a \end{bmatrix} + \text{Higher Order Terms,}$$

$$\tag{11}$$

where u_a and v_a are wind speeds in $x-$ and $y-$ direction, likewise u_i and v_i are sea ice velocities. The linearisation is performed around $[u_i, v_i] = 0$. The first term on LHS in Eq. 11 is the constant term which represents the energy transferred to the sea ice and the first-order terms are the dissipative component from the relative movement between sea ice and winds. The dissipation loss due to this component is given by an expression similar to Eq. 10 and computed as:

$$E'_{ai} = \left(-2\rho_a C_a \sqrt{u_a^2 + v_a^2} \begin{bmatrix} \delta u_i \\ \delta v_i \end{bmatrix} \right.$$
$$\left. + \frac{\rho_a C_a (u_a \delta v_i - v_a \delta u_i)}{\sqrt{u_a^2 + v_a^2}} \begin{bmatrix} -v_a \\ u_a \end{bmatrix} \right) \cdot \begin{bmatrix} \delta u_i \\ \delta v_i \end{bmatrix}, \tag{12}$$

where E'_{ai} is the energy loss from the first-order terms of the air-ice drag, δu_i and δv_i are the sea ice velocities around the mean. And, similar to the bottom friction energy loss, the time-average of this energy loss is given by $\overline{E''_{ai}}$.

To evaluate the dissipation on subdaily motion of sea ice, the point model derived subdaily sea ice motion δu and δv, which we obtained by removing the low frequency mean drift, is used as the δu_i and δv_i. These are obtained from the reference model runs (Figs. 4 and 5).

Using these ice velocities and the same values for parameters ρ_a and C_a as given in Section 3, the above energy dissipation Eq. 12 and its time average are computed for constant winds (u_a and v_a) with varying magnitude for all the beacons.

The winds are assumed to be blowing 45 ° North-East with varying constant wind speeds from 1 m/s to 32 m/s scaled by a factor of 2. It is seen that (Fig. 13) increasing the wind naturally increases the dissipation which, for a speed of 8 m/s is around $2-3\%$ of the loss of energy to the bottom frictional stress for all the beacons except beacon 13. This dissipation becomes quite significant for a wind speed of 32 m/s with values ranging from $10-20\%$ of the loss to the bottom frictional stress for all beacons except, again beacon 13. Beacon 13 is an exception here because in this case the bottom friction energy loss is in itself very low. This could be a result of extremely low tidal amplitudes along this beacon trajectory (Figs. 2, 6g and h). Thus, it can be said that in this dataset of the Barents Sea region, on a subdaily scale the non-linear wind drag can cause dissipation at the air-ice interface where this effect increases with increasing wind speeds. In comparison to energy loss of tides to bottom friction, this effect is observed to be not very high for normal wind speeds of around 8 m/s.

Such a dissipation due to winds without any subdaily signal can in turn, affect the subdaily sea ice oscillations. In the case of the beacon dataset the wind speeds were low enough for this dissipation to be low. But in case there is a storm surge which does not have any subdaily signal, there is a chance that the sea ice subdaily motion might be affected due to the dissipation term seen in Eq. 11. Although, the evaluation above is for the beacon dataset, the procedure is valid for any other buoy dataset and can help evaluate the significance of wind stress on a subdaily scale.

6.2 Dissipation at ice-tide interface

The interfacial dissipation due to water-ice tidal drag is evaluated, where the expression of the corresponding energy loss is given by:

$$E_{wi} = -\boldsymbol{\tau}_{wit} \cdot (\boldsymbol{u}_{wt} - \boldsymbol{u}_{it}), \tag{13}$$

$$E_{wi} = -\rho_w C_w |\boldsymbol{u}_{wt} - \boldsymbol{u}_{it}| (\boldsymbol{u}_{wt} - \boldsymbol{u}_{it}) \cdot (\boldsymbol{u}_{wt} - \boldsymbol{u}_{it}),$$
$$\overline{E_{wi}} = -\rho_w C_w \overline{|\boldsymbol{u}_{wt} - \boldsymbol{u}_{it}|^3}, \tag{14}$$

where E_{wi} is the energy loss from the tidal part of the water-ice drag, $\boldsymbol{\tau}_{wit}$ is the water-ice drag from the tidal component only, $\boldsymbol{u}_{wt}$ is the tidal velocity, $\boldsymbol{u}_{it}$ is the reference point model-derived sea ice oscillations obtained by removing the mean drift from model runs and a time-average given by $\overline{E_{wi}}$.

For a quantitative analysis, the comparison between this dissipation ($\overline{E_{wi}}$) and time-averaged loss to bottom friction ($\overline{E_b}$) is seen in Fig. 14.

The average energy loss between the sea ice and tidal interface (blue dots) is just around $2-3\%$ of the loss of energy of tides to the bottom friction for all the beacons except beacon 13. Again, beacon 13 is an exception because of the lower tides along its trajectory. Thus, we conclude that in the beacon dataset the drag from the tides is the major cause of sea ice oscillations yet the dissipation between the sea ice and tide interface is negligible. This conclusion holds true under the condition that no storm surges are present and the winds have very low subdaily signals.

The analyses presented here relied on the point model simulations which in turn relied on external datasets i.e. ERA5, CMEMS and GTSM. There are no data on the uncertainty of these datasets in this region of the Barents Sea or near marginal ice zones. Yet to evaluate the consistency of our conclusions we did a sensitivity analysis on the results of our two analyses presented above by using other datasets than the three mentioned above. It was seen that the results of the two analyses we presented here were not very sensitive to the external datasets
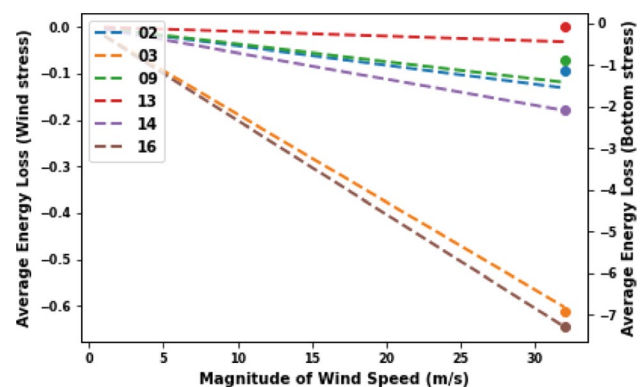
Fig. 13 Time-averaged energy loss computed using Eq. 12 plotted against varying wind speed magnitudes. The dots correspond to time-averaged bottom energy loss for respective beacons with their values corresponding to the right vertical (y-) axis. The different coloured lines correspond to each beacon and the same colour of respective beacon is used to represent the time-averaged energy loss to the bottom friction

and as such, the conclusions remained consistent. Details of this sensitivity analysis can be found in Online Resource 4.

Now, we started off with the problem that in shallow water regions it is not clear if the dissipation at the ice and water interface is negligible on a tidal/subdaily scale. Through our study, it is clear that the ice-water tidal drag plays a significant role in sea ice oscillations, yet the role of dissipation at the ice-tide interface is negligible. Furthermore, the effect of bottom frictional drag in inducing a relative difference in ice and water velocities is low for our dataset. This conclusion is only valid for the current dataset. Yet, the hypothesis presented in Section 5.2 depends on the free drift and tidal equations for range of depths. So, we can hypothesise that the conclusion above is also valid for many other areas, which can be proved with the methodology used in the paper if a valid dataset is available for these areas.

7 Summary and conclusions

Sea ice and its interaction with tides is one of the major challenges for global hydrodynamic tidal models (Stammer et al. 2014). The presence of sea ice leads to a dissipation of tidal energy and most existing global tidal models include this by adding a dissipative term similar to the bottom friction term while assuming a stationary sea ice cover. However, in reality, the sea ice cover varies over the year and sea ice is drifting. Added to this, the nature of frictional dissipation due to drifting sea ice is partly unknown.

In this paper we aim to estimate the significance of the frictional dissipation due to free drifting sea ice. There is little to no frictional dissipation between free drift sea ice and tides for deeper and open oceans. But for shallow water regions, the bottom friction plays a role and as such, the dissipation in such a case is not known. To study this, a dataset of beacon trajectories in the Barents Sea region showing subdaily sea ice oscillations is used. Along with the dataset, a physics-based point sea ice model was developed which tracked the beacon trajectories and was forced with external data from an ocean model, a tidal model, and an atmospheric model (Table 1). The spectrum of the subdaily oscillations showed that model and observations were in good agreement and that the M_2 tidal signal was the dominant one in the oscillations, but in this region, the Coriolis frequencies are also very close to the M_2 frequency.

Two analyses were done to evaluate the nature of the dissipation in this Barents Sea dataset. In the first analysis, a direct and strong relationship was observed between the sea ice oscillations from the observations and the tides and also between the observations and the model. This suggests that the observations had a large tidal signal and sea ice and tides

move together. So the dominance at M_2 frequency in the spectrum is highly correlated to the tidal currents.

Next, we studied the causality and physical processes using sensitivity tests on the forcing in the model. It was noted that the oscillations are a result of the inertial forcing due to wind (air-ice) drag, the water-ice drag from tidal currents and the pressure gradients from the tidal sea surface heights. In our study, the effect of water-ice drag from tidal currents dominated the forcing and the influence of the tidal pressure gradients and the inertial (from air-ice drag) terms was comparatively low. This may be more balanced in deeper waters. Thus, based on the conclusions of the two analyses — tides and sea ice are strongly connected and the drag from the tidal currents being the main cause of oscillations — we can say that the sea ice follows the tides.

The dissipation between sea ice and tides was further evaluated for all the beacons (Fig. 14) by computing the time-averaged energy loss and comparing it to the bottom friction energy loss of tides. It is seen that the dissipation is just $2-3\%$ of the equivalent bottom frictional energy loss of tides. Thus, we concluded that the tides do not have significant dissipation due to the free drift sea ice in this dataset of Barents Sea region. This implied that the bottom frictional stress from the shallower Spitsbergen Shelf does not induce significant differences between the tidal and sea ice velocities, and as such, the dissipation remains negligible.

This conclusion corresponds to the experiment in the Barents Sea region where, at the time, ERA5 data showed that the winds had low speed and no subdaily signals in them. It was seen in the sensitivity analysis that if the winds had a strong subdaily signal then the above conclusion might not hold true as the sea ice oscillations will have a large inertial part too. Further, for the case of strong winds with no tidal signals we studied the effect of a non-linear air-ice drag term on sea ice oscillations in the beacon dataset. This effect was observed to be around $2-3\%$ of equivalent bottom friction
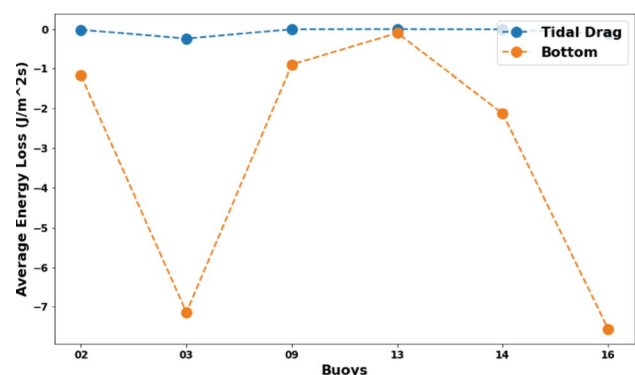
Fig. 14 Total average energy loss or gain of tides over the entire beacon trajectory (which is averaged over M_2 tidal period) is plotted for all the beacons. For comparison a loss of energy to sea bed bottom friction stress is used as a reference

energy loss for wind speed of 8 m/s but increasing to around 20% for strong constant wind of 32 m/s. Hence, stronger winds such as in the case of storm surges can also have some impact on subdaily sea ice oscillations and this should be evaluated for each region and time separately.

Based on the mathematical analysis, we hypothesise that the similar conclusion of negligible dissipation between free drift sea ice and tides might hold true for other areas of the Arctic. To verify this, one would need more of such beacon observations in other areas in the free drift regime and for different time periods. The methodology presented here, is, in principle, applicable to any such dataset. Given this, for global tidal and storm surge models the dissipation from free drift sea ice on tides should be evaluated on a case-by-case basis. For deeper open oceans with low winds it can be said that the dissipation from such ice is negligible. But for shallow water regions with varying wind conditions this dissipation needs to be evaluated based on local observations and the methodology presented here.

In this paper, we have not studied the dissipation due to sea ice drifting under strong internal stresses. Some analysis was done on sea ice drifting under strong internal stresses for the beacon dataset above the 78 °N latitude but it was inconclusive as the dataset was too scarce. Hibler et al. (2006) saw amplification in the sea ice oscillation spectrum from the tides+winds forcing for the Arctic Central Basin, but this could very well be local and seasonal. It is expected that the internal stresses will dampen the sea ice oscillations. Hence, the resulting sea ice velocities will be different than the tidal velocities, which will imply that the dissipation will be more. But the nature of this dissipation is not known and will be part of future study. It thus, remains to be seen what is the interaction between such sea ice drifting under strong internal stresses and tides and the resulting quantitative nature of the dissipation.

Declarations

Conflicts of interest The authors have no conflict of interest

References

Beitsch A, Kaleschke L, Kern S (2014) Investigating high-resolution AMSR2 sea ice concentrations during the february 2013 fracture event in the beaufort sea. Remote Sensing 6(5):3841–3856. https://doi.org/10.3390/RS6053841

Brown RA (1981) Modeling the geostrophic drag coefficient for AIDJEX. Journal of Geophysical Research: Oceans 86(C3):1989–1994. https://doi.org/10.1029/jc086ic03p01989

Chen C, Gao G, Qi J, Proshutinsky A, Beardsley RC, Kowalik Z, Lin H, Cowles G (2009) A new high-resolution unstructured grid finite volume Arctic Ocean model (AO-FVCOM): An application for tidal studies. J Geophys Res 114(C8), https://doi.org/10.1029/2008JC004941

Copernicus Marine Service (2014) Global Ocean 1/12° Physics Analysis and Forecast. https://doi.org/10.48670/moi-00016

Dmitriev NE, Proshutinsky AY, VlNJE T, Yu A, Yu Proshutinsky A, Scienr A (1991) Tidal ice dynamics in the area of Svalbard and Frans Josef Land. Polar Research 9(2):193–205. https://doi.org/10.3402/POLAR.V9I2.6791

Furevik T, Foldvik A (1996) Stability at M2 critical latitude in the Barents Sea. Journal of Geophysical Research: Oceans 101(C4):8823–8837. https://doi.org/10.1029/96JC00081

Gjevik B, Straume T (1989) Model simulations of the M_2 and the K_1 tide in the Nordic Seas and the Arctic Ocean. Tellus A 41A(1):73–96. https://doi.org/10.1111/j.1600-0870.1989.tb00367.x

Heil P, Hibler WD (2002) Modeling the High-Frequency Component of Arctic Sea Ice Drift and Deformation. J Phys Oceanogr 32:3039–3057

Hersbach H, Bell B, Berrisford P, Biavati G, Horányi A, Muñoz Sabater J, Nicolas J, Peubey C, Radu R, Rozum I, Schepers D, Simmons A, Soci C, Dee D, Thépaut JN (2018) ERA5 hourly data on single levels from 1979 to present. https://doi.org/10.24381/cds.adbb2d47

Hibler ID, Roberts A, Heil P, Proshutinsky AY, Simmons HL, Lovick J (2006) Modeling M2 tidal variability in Arctic sea-ice drift and deformation. Annals of Glaciology 44:418–428. https://doi.org/10.3189/172756406781811178

Hunkins K (1967) Inertial oscillations of Fletcher's Ice Island (T-3). Journal of Geophysical Research 72(4):1165–1174. https://doi.org/10.1029/jz072i004p01165

Kagan BA, Sofina EV (2010) Ice-induced seasonal variability of tidal constants in the Arctic Ocean. Continental Shelf Research 30(6):643–647. https://doi.org/10.1016/j.csr.2009.05.010

Kaleschke L, Müller G (2022) Sea ice drift from autonomous measurements from 15 buoys, deployed during the IRO2/SMOSIce field campaign in the Barents Sea March 2014. PANGAEA. https://doi.org/10.1594/PANGAEA.941334

Kaleschke L, Tian-Kunze X, Maaß N, Beitsch A, Wernecke A, Miernecki M, Müller G, Fock BH, Gierisch AMU, Heinke Schlünzen K, Pohlmann T, Dobrynin M, Hendricks S, Asseng J, Gerdes

R, Jochmann P, Reimer N, Holfort J, Melsheimer C, Heygster G, Spreen G, Gerland S, King J, Skou N, Søbjaerg SS, Haas C, Richter F, Casal T (2016) SMOS sea ice product: Operational application and validation in the Barents Sea marginal ice zone. Remote Sensing of Environment. https://doi.org/10.1016/j.rse.2016.03.009

Kleptsova O, Pietrzak JD (2018) High resolution tidal model of Canadian Arctic Archipelago, Baffin and Hudson Bay. Ocean Modelling 128:15–47. https://doi.org/10.1016/j.ocemod.2018.06.001

Kowalik Z (1979) A note on the co-oscillating M2-tide in the Arctic Ocean. Deutsche Hydrographische Zeitschrift 32(3):100–112. https://doi.org/10.1007/BF02226997

Kowalik Z (1981) A study of the M-2 tide in the ice-covered arctic ocean. Modeling, Identification and Control: A Norwegian Research Bulletin 2(4):201–223. https://doi.org/10.4173/mic.1981.4.2

Kowalik Z, Proshutinsky AY (1994) The arctic ocean tides. American Geophysical Union (AGU). https://doi.org/10.1029/gm085p0137

Kowalik Z, Untersteiner N (1978) A study of the M2 tide in the Arctic Ocean. Deutsche Hydrographische Zeitschrift 31(6):216–229. https://doi.org/10.1007/BF02226539

Lammert A, Brümmer B, Kaleschke L (2009) Observation of cyclone-induced inertial sea-ice oscillation in Fram Strait. Geophys Res Lett 36(10), https://doi.org/10.1029/2009GL037197

Leppäranta M, Leppäranta M (2011a) Equation of drift ice motion. In: The Drift of Sea Ice, Springer: Berlin, pp 143–184, https://doi.org/10.1007/978-3-642-04683-4_5

Leppäranta M, Leppäranta M (2011b) Free drift. In: The Drift of Sea Ice, Springer: Berlin, pp 185–212, https://doi.org/10.1007/978-3-642-04683-4_6

Leppäranta M, Omstedt A (1990) Dynamic coupling of sea ice and water for an ice field with free boundaries. 42(4):482–495. https://doi.org/10.3402/TELLUSA.V42I4.11892

Mahoney AR (2018) Landfast Sea Ice in a Changing Arctic. Tech. rep., https://arctic.noaa.gov/Report-Card/Report-Card-2018/ArtMID/7878/ArticleID/788/Landfast-Sea-Ice-in-a-Changing-Arctic

McPhee MG (1978) A simulation of inertial oscillation in drifting pack ice. Dynamics of Atmospheres and Oceans 2(2):107–122. https://doi.org/10.1016/0377-0265(78)90005-2

McPhee MG (1980) An analysis of pack ice drift in summer. In: Sea ice processes and models, University of Washington Press, pp 62–75

McPhee MG (1982) Sea ice drag laws and simple boundary layer concepts, including application to rapid melting, report 82-4 edn. CRREL report ; 82-4, United States Army Cold Regions Research and Engineering Laboratory, Hanover, N.H

Middleton JH, Denniss T (1993) The propagation of tides near the critical latitude. Geophysical and Astrophysical Fluid Dynamics 68(1–4):1–13. https://doi.org/10.1080/03091929308203559

Muis S, Verlaan M, Winsemius HC, Aerts JC, Ward PJ (2016) A global reanalysis of storm surges and extreme sea levels. Nature Communications 2016 7(1):1–12. https://doi.org/10.1038/ncomms11969

Müller M, Cherniawsky JY, Foreman MG, Von Storch JS (2014) Seasonal variation of the M 2 tide. Ocean Dynamics 64(2):159–177. https://doi.org/10.1007/s10236-013-0679-0

Omstedt A (1980) A sensitivity analysis of steady, free floating ice. (RMK, Rapport Meteorologi och Klimatologi) SMHI Retrieved from https://www.urnkbse/resolve?urn=urn:nbn:se:smhi:diva-2732

Omstedt A, Nyberg L, Leppäranta M (1996) On the ice-ocean response to wind forcing. Tellus, Series A: Dynamic Meteorology and Oceanography 48(4):593–606. https://doi.org/10.3402/tellusa.v48i4.12145

Padman L, Erofeeva S (2004) A barotropic inverse tidal model for the Arctic Ocean. Geophys Res Lett 31(2), https://doi.org/10.1029/2003GL019003

Pease CH, Salo SA, Overland JE (1983) Drag measurements for first-year sea ice over a shallow sea. J Geophys Res: Oceans 88(C5):2853–2862. https://doi.org/10.1029/JC088IC05P02853@10.1002/(ISSN)2169-9291.ICEZONE1

Pease CH, Turet P, Pritchard RS (1995) Barents Sea tidal and inertial motions from Argos ice buoys during the Coordinated Eastern Arctic Experiment. J Geophys Res 100(C12):24705–24718. https://doi.org/10.1029/95jc03014

Stammer D, Ray RD, Andersen OB, Arbic BK, Bosch W, Carrère L, Cheng Y, Chinn DS, Dushaw BD, Egbert GD, Erofeeva SY, Fok HS, Green JAM, Griffiths S, King MA, Lapin V, Lemoine FG, Luthcke SB, Lyard F, Morison J, Müller M, Padman L, Richman JG, Shriver JF, Shum CK, Taguchi E, Yi Y (2014) Accuracy assessment of global barotropic ocean tide models. Rev Geophys 52(3):243–282. https://doi.org/10.1002/2014RG000450

Steele M, Zhang J, Rothrock D, Stern H (1997) The force balance of sea ice in a numerical model of the Arctic Ocean. J Geophys Res 102(C9):61–82. https://doi.org/10.1029/97JC01454

Bij de vaate I, Vasulkar A, Slobbe C, Verlaan M (2020) The influence of Arctic fast ice cover on seasonal modulation of the M2 tide. Journal of Geophysical Research: Oceans Submitted

Verlaan M, De Kleermaeker S, Buckman L (2015) GLOSSIS: Global storm surge forecasting and information system. In: Australasian Coasts & Ports Conference 2015: 22nd Australasian Coastal and Ocean Engineering Conference and the 15th Australasian Port and Harbour Conference. Engineers Australia and IPENZ, Auckland, New Zealand, pp 229–234

Zubov N (1945) Ldy Arktiki. Izdatelstvo Glavsermorputi, Moscow, p 360. English translation 1963 by US Naval Oceanographic Office and American Meteorological Society, San Diego